FORSCHUNGSZENTRUM ROSSENDORF
Mitglied der Wissenschaftsgemeinschaft Gottfried Wilhelm Leibniz

WISSENSCHAFTLICH-TECHNISCHE BERICHTE
FZR-393
Dezember 2003
ISSN 1437-322X

Eberhard Altstadt, Helmar Carl and Rainer Weiss

Fluid-Structure Interaction Investigations for Pipelines

Herausgeber:
Forschungszentrum Rossendorf e.V.
Postfach 51 01 19 · D-01314 Dresden
Telefon +49 351 26 00 · Telefax +49 351 2 69 04 61
http://www.fz-rossendorf.de/

Als Manuskript gedruckt

FORSCHUNGSZENTRUM ROSSENDORF
WISSENSCHAFTLICH-TECHNISCHE BERICHTE
FZR-393
Dezember 2003

Eberhard Altstadt, Helmar Carl and Rainer Weiss

Fluid-Structure Interaction Investigations for Pipelines

Fluid-Structure Interaction Investigations for Pipelines

Eberhard Altstadt, Helmar Carl and Rainer Weiss

Forschungszentrum Rossendorf
Institute of Safety Research

Contents

Abbreviations and symbols

A	cross section area
BP	bouncing plate
c_F	sound speed of fluid
CWHTF	cold water hammer test facility
D	diameter
DOF	Degree of freedom
E	elasticity modulus (Young's modulus)
eq	Equation
FSI	fluid-structure interaction
$dH = H_1 - H_0$	evacuation height
K	bulk modulus
m_B	mass of the bouncing plate
MP*x*	measuring position x = 1 … 10
p_1	evacuation pressure
p_3	pressure in the vessel
p_{max}	amplitude of the pressure wave in the water
$\hat{p}$	Pressure peak
s	wall thickness or second
t	time
t_c	condensation time of the steam volume below the bouncing plate
T_0	time period
t_{open}	valve opening time
u	displacement
u_c	common displacement of fluid front and bouncing plate at $t = t_0 + t_c$
v	velocity
v_c	initial velocity of the bouncing plate after bouncing
v_{F0}	initial fluid velocity
ϵ_a, ϵ_t	axial strain, tangential strain
ρ	density
ρ_F, ρ_P	fluid density, pipe wall density
σ_a, σ_t, σ_e	axial stress, tangential stress, equivalent stress
ν	Poisson number
$()_F$	Fluid (used indices)
$()_B$	bouncing plate (used indices)

1 Introduction

In existing Nuclear Power Plants water hammers can occur in case of an inflow of sub-cooled water into pipes or other parts of the equipment, which are filled with steam or steam-water mixture. They also may appear as the consequence of fast valve closing or opening actions or of breaks in pipelines, with single phase or two-phase flow. In the latter case, shock waves in two-phase flow must be expected. In all cases, strong dynamic stresses are induced in the wall of the equipment. Further, the change of the momentum of the liquid motion and the deformation of the component due to the dynamic stresses generate high loads on the support structures of the component, in which the water hammer respectively the shock wave occurs.

The influence of the fluid-structure interaction on the magnitude of the loads on pipe walls and support structures is not yet completely understood. In case of a dynamic load caused by a pressure wave, the stresses in pipe walls, especially in bends, are different from the static case. The propagating pressure wave may cause additional non-symmetric deformations which increase the equivalent stresses in comparison to the symmetric load created by a static inner pressure. On the other hand, fluid-structure interaction causes the structure to deform, which leads to a decrease of the resulting stresses. The lack of experimental data obtained at well defined geometric boundary conditions is a significant obstacle for the validation of codes which consider fluid-structure interaction. Furthermore, up to now the feedback from structural deformations to the fluid mechanics has not been fully implemented in existing calculation software codes. Therefore, at FZR a cold water hammer test facility (CWHTF) was designed and built up.

2 The cold water hammer test facility

The CWHTF consists of a pressure vessel (tank), a pipeline with two straight sections (one horizontally and one vertically oriented), two 90° bends (curvature radius 306 mm) and a fast opening valve. The total length of the pipeline is about 3 meters, the outer pipe diameter is about 219 mm and the wall thickness 6 mm. The vertical pipe region is terminated by a lid flange which acts as a bouncing plate. Figure 1 shows the principal design of the facility.

The water hammer is generated by the accelerated water bouncing against the lid flange. The water level in the vertical part of the pipeline is adjusted in a certain distance from the lid flange. This free volume above this level is evacuated ($p_1 << 1$ bar) through a hole in the bouncing plate. During this time the fast acting valve is closed. After the fast opening of the valve the fluid is accelerated until bouncing against the upper lid of vertical pipeline. At that time a water hammer is induced. The pressure in the tank p_3 may be increased by pressurized air (up to 5 bar) to increase the amplitude of the pressure waves generated. The generated pressure wave travels back through the bend, causing a strong structural response of the pipe system.

The valve is connected to a spring mechanism which allows the quick opening of the turning plate within a defined time. The turning plate is supported in the horizontal middle plane of the pipe. The opening time can be varied between 0.02 s and 0.2 s by changing the pre-stress of the springs. The opening mechanism is hydraulically initiated by loosening the arrest of the pre-stressed springs. This makes no counterthrust onto the pipe system, so the excitation of vibrations is rather low. Table 1 contains the main parameters of the pipe and of the vessel:

Table 1: Main parameters of the CWHTF		
Parameter	**Pipeline**	**Vessel**
Outer diameter	219 mm	800 mm
Wall thickness	6.0 mm	6.0 mm
Curvature radius of the bend	306 mm	-
Total pipe length L_0	3.285 m	-
Internal volume	124 litres	750 litres
Design pressure	60 bar	10 bar
Pressure of plastification	90 bar	-
Pressure of break	226 bar	-

2.1 Instrumentation

The pipeline is instrumented with a lot of different sensors between the lid flange and the valve (fig. 2). Dynamic pressures, strains, void fractions and acceleration can be measured. Needle probes measure the conductivity of the medium at its tip. Therefore, their signals give information about position and velocity of the water front during the acceleration phase (before the water hammer occurs). The dynamic pressure sensors detect the pressure change at the inner side of the pipe wall. The acceleration sensors measure the motion of the pipeline at the bouncing plate in 3 spatial directions. Strain gauges are mounted at 7 axial locations of the outer surface of the pipeline. At each axial location there are at least two pairs of strain gauges (one axially and one tangentially oriented gauge per pair) at the circumferential positions 0° and 180°. The maximum sampling frequency is 10 kHz for all signals. The measurements are performed at room temperature.

2.2 Estimation of pressure amplitudes of the water hammer

Some test parameters can be varied to initiate different pressure amplitudes of the water hammer (shown in table 2).

Table 2: Variation of the test parameters	
Evacuation pressure	23 mbar ..... 1 bar
Evacuation height	0.15 m ..... 1.2 m
Valve opening time	0.02 s .... 1 s
Pressure in the vessel	1 bar ..... 5 bar

To estimate the bouncing velocity and the amplitude of the initiated pressure wave a 1D numerical model for the acceleration phase was developed which based on the following assumptions:

- incompressible, frictionless fluid (density)
- one dimensional velocity field (constant over cross section)
- evacuation pressure in the free volume remains constant until the impingement of the fluid front

Figure 1 shows the geometrical and physical quantities used in the model equations. The momentum balances for pipe and vessel lead to a second order differential equation for the motion of the fluid front z:

$$\ddot{z}\cdot[L_0+\alpha\cdot H_2+(1-\alpha^2)\cdot z]+\dot{z}^2\cdot(1-\alpha^2)+g\cdot[H_0-H_2+(1+\alpha)\cdot z] = \frac{1}{\rho}\cdot[p_3(t)-p_1-\Delta p_V(t)] \qquad \textbf{Eq. 1}$$

$$z(0)=0; \qquad \dot{z}(0)=0; \qquad \alpha=D_{pipe}/D_{vessel}$$

This equation is solved with a 4th order Runge-Kutta algorithm after transforming it into a system of two 1st order equations. As a result of this simulation the bouncing velocity and the time from valve opening till fluid impingement are calculated. The pressure amplitude can then be estimated from the extended Joukowsky formula.

Table 3 shows the maximum values which can be expected with different test parameters.

Table 3: Bouncing velocity and pressure amplitude in dependence on evacuation height and vessel pressure (valve opening time 0.02 s)

Evacuation height H_1- H_0	Vessel pressure $p_{3,0}$	Bouncing velocity	Pressure amplitude
0.155 m	1 bar (open)	2.97 m/s	36.5 bar
1.20 m	1 bar	7.35 m/s	91 bar
1.20 m	5 bar	17.1 m/s	212 bar

The values for the velocity and the pressure amplitude are upper limits since the assumptions made in the beginning of this section are not fulfilled. Furthermore this simulation does not consider the global FSI effects resulting from the bending flexibility of the pipeline (junction coupling). Additionally the simulations showed that for small values of the valve opening time the bouncing velocity is constant, only if the opening time exceeds a critical value the bouncing velocity is reduced. The critical opening time depends on the other test parameters such as evacuation height and vessel pressure. Up to an opening time of 0.02 s ... 0.03 s there is only an insignificant reduction of the bouncing velocity even for short acceleration phases.

3 Water hammer experiments

The first experiments were carried out with an open vessel (i.e. $p_3(t) = 1$ bar = const) at room temperature (fig. 8). The water level in the vertical pipe and in the vessel (before evacuation) varied between 0.15 m and 0.8 m for the different test series. The valve opening time was some 0.0265 s. The free volume beneath the bouncing plate was evacuated to evaporation pressure (p_1 = 0.023 bar). A sampling frequency of at least 5 kHz is necessary to see the dynamic effects and to get reproducible results. With an evacuation height of 0.155 m a pressure amplitude of some 25 bar was obtained in that experiment.

The time between trigger (start of valve opening) and bouncing (initiation of the water hammer) is about 110 ms. This fits very well to the pre-calculation using the model of section 4 (tend = 104 ms). The bouncing velocity is predicted quite well by the model, whereas the pressure amplitude is over-estimated by some 30-50% since the effect of the junction coupling is not included.

After the main pressure wave has worn off some additional smaller pressure peaks occur. This hints to cavitation due to the sub-pressure in the reflection phase of the main pressure wave. The circumferential strains are in the linear-elastic range. As expected in the straight pipe they follow the pressure signal. In the pipe bend range an ovalization of the cross section occurs,

consequently at the intrados position (0°) and the extrados position (180°) circumferential tension is observed, whereas at the 270° position circumferential pressure strain is detected at outer wall surface. Due to the junction coupling effect the pipe system is excited to vibrations by the bouncing fluid what is also clearly visible in the acceleration signals and in the strain signals of the pipe bend. In the pipe bend the strain amplitudes caused by junction coupling are higher than those ones caused by the pressure wave itself. Figure 8 shows e.g. the pressure at a measuring position 100 mm below the bouncing plate (cf. fig. 1) and the acceleration of the bouncing plate. A 3D finite element model is developed which simulates the coupled pressure wave in the fluid and the stress wave in pipe wall. This model also includes the junction coupling due to the bouncing process. The simulation results are used to give a detailed interpretation of the measurements.

3.1 Preliminary investigations

3.1.1 Modal analysis test

The modal test at the CWHTF was performed without water. An impact hammer with a mass of 300 g and a rubber tip was used to generate the excitation. The impact was applied to the bouncing plate of the CWHTF in vertical direction. The out of plane modes of the pipe were not excited since they are not important from the viewpoint water hammers. Acceleration signals were measured at MP9 (x,y,z), MP2 (x,z), MP10(x,z) and MPF(x,z). Fig. 3 shows the accelerations over the time at MP9 and fig. 4 shows the according transfer functions. The commercial software package STAR-struct® was used to extract the natural frequencies and mode shapes from the measurement signals [1]. The algorithm for frequency and mode extraction is based on the phase separation technique which is described for example in [2].

The natural frequencies of the CWHTF filled with water can be calculated from the frequencies of the empty CWHTF by using the effective structural density (the mass of the internal fluid is added to the pipe mass). The effective structural density can be calculated by

$$\rho_{eff} = \rho_P + \rho_F \cdot \frac{A_F}{A_P} \qquad \textbf{Eq. 2}$$

The corrected natural frequency follows from

$$f_{filled} = f_{empty} \cdot \sqrt{\frac{\rho_P}{\rho_{eff}}} = \frac{f_{empty}}{\sqrt{1 + \frac{\rho_F \cdot A_F}{\rho_P \cdot A_P}}} \qquad \textbf{Eq. 3}$$

where A_P is the cross section of the pipe wall, A_F the internal cross section of the pipe (fluid cross section), ρ_F the fluid density and ρ_P the pipe wall density. For the CWHTF pipe the ratio f_{filled}/f_{empty} is about 0.70. The figures 5-7 show the mode shapes 1-3. There are additional peaks visible in the spectra (fig. 4) at 36 Hz, 40 Hz, 48 Hz and 55 Hz. These frequencies belong to the out-of-plane modes which are not listed in table 2. Above 100 Hz there are no significant global vibrations.

Table 4: Natural frequencies of the CWHTF structure (in-plane up to 100Hz)			
Mode	natural frequency empty	natural frequency filled	Mode shape
1	13.35 Hz	9.3 Hz	1st in-plane bending mode, vertical and horizontal pipe in-phase
2	44.13 Hz	30.6 Hz	2nd in-plane bending mode, vertical and horizontal pipe anti-phase
3	89.04 Hz	62 Hz	3rd in-plane bending mode

3.1.2 Water hammer pre-tests

A series of water tests was performed to verify the functionality of the CWHTF and of the measuring data recording system. In these pre-tests a somewhat different instrumentation was used than during the main tests (chapter 3.2). Acceleration sensors and conductivity probes were additionally used whereas the number of strain and pressure sensors was reduced.

The results of these pre-tests are summarized in [3]. It was shown that the analytical 1D-model for the acceleration phase [3] can predict the bouncing velocity quite well. The estimation of the pressure amplitude based on the extended Joukowsky equation is of course too conservative, since global elasticity effect (e.g. junction coupling) is not considered. Figures 8 and 9 show all types of signals (valve opening, conductivity, pressure, acceleration and strain) to illustrate the course of the events during a water hammer test and to give an impression of the order of magnitude of the different signals. As a result of the observations in the pre-tests the fixing of the vessel support and of the valve at the foundation had to be reinforced to avoid loosening.

3.2 Experiments

3.2.1 Overview about performed experiments

For each test all measuring positions were recorded with a sampling frequency of 10 kHz. Four channels could be recorded at once (including the trigger signal). In general, each of the 17 tests consists of 8 shots with identical test parameters. Table 5 shows an overview about the performed tests.

Table 5: Experiments performed at the CWHTF 06/2001 - 09/2001						
Folder name (Date of test)	Evacuation height $H_1 - H_0$ [m]	Valve opening time t_{open} [s]	Evacuation pressure p_1 [mbar]	Fixation of the bouncing plate	Gas pressure in the vessel p_3 [bar]	measured pressure amplitude p_{max} [bar]
150601	0.15	0.021	29	fixed (old)	1	32.5
150601a			40			29
150601b			50			27
190601	0.3	0.021	29	fixed (old)	1	44
190601a			40			41
190601b			50			38
210601	0.8	0.021	29	fixed (old)	1	67.5
270601			29	fixed (new)		68
270601b			50			50
290601	0.3	0.021	29	free	1	41
300601	0.15	0.021	29	free	1	31
010701					3	53
020701					5	67
030701	0.15	0.021	29	fixed (new)	5	82
040701	0.30	0.021	29	fixed (new)	3	84
040701a					5	106
210901	0.15	0.029	25	fixed (new)	1	33
210901a		0.5				28
210901b		> 1				5
210901c	0.15	0.029	25	fixed (new)	1	0 [1]; 32

[1] Pressure sensor K22 isolated from the water (only measurement of accelerating sensitivity)

In all tests the initial water level in the pipe H_0 and the water level in the vessel H_2 was equal. The deviation between the planned test program [4] and the tests performed are caused by the following reasons:

1. The minimal possible evacuation pressure was 25 mbar, caused by temperature of the water
2. The maximum evacuation height was 0.8 m (to prevent damage from the CWHTF), the foundation of the building allowed only pressure amplitudes up to 100 bar (a force of 400 kN acts for a short time)
3. Some experiments were repeated because of changing of the fixation of the bouncing plate (old fixation was damaged during the first 3 experiments)
4. Valve opening times of 200 ms could not be realised. Instead there were experiments with valve opening times from 500 ms to more than 1 s.

The planned tests with evacuation height 1.2 m were not carried out since the valve fixation and anchoring to the foundation would have been destroyed. Even in the tests performed with an evacuation height of H_1-H_0 = 0.8 m and without over pressure in the vessel some damaging was observed.

3.2.2 Measuring signals

Table 6 shows the assignment of measuring positions (fig.2) and the channels of the data recording system (PK-System). The sampling frequency is 10 kHz for each channel. Four channels can be simultaneously recorded.

Table 6: Channels and measuring quantities

Channel	Measuring position	Definition	Channel	Measuring position	Definition
K1	MP1	MP1-D-0-T	K11	MP5	MP5-D-180-T
K2		MP1-D-0-A (def)	K12		MP5-D-180-A
K22		MP1-P-90	K13		MP5-D-270-T
K3		MP1-D-180-T	K14		MP5-D-270-A
K4		MP1-D-180-A	K15	MP6	MP6-D-0-T
K23	MP2	MP2-P-90	K16		MP6-D-0-A (def)
K5	MP3	MP3-D-0-T	K17		MP6-D-180-T
K6		MP3-D-0-A	K18		MP6-D-180-A
K24		MP3-P-90	K19		MP6-D-270-T
K7		MP3-D-180-T	K20		MP6-D-270-A
K8		MP3-D-180-A	K26	MP7	MP7-P-0
K25	MP4	MP4-P-90	K27		MP7-P-90
K9	MP5	MP5-D-0-T	K28		MP7-P-180 (def)
K10		MP5-D-0-A	K21	Valve	Trigger

Legend: D - strain; P - pressure; A - axial; T - tangential;
0,90,180,270 - azimuthal position in degrees (0° = intrados, 180° = extrados)

Channel K21 is always recorded as trigger signal. It is used for the determination of the valve opening time and for the synchronization of signals from different measurements with identical test parameters. Channels 2, 16 and 28 were defect during some of the measurements.

The pressure is measured by dynamic piezoelectric sensors, the strains by strain gauges. Table 7 shows the sensor properties for the measuring channels. The strain gauge circuit is a half bridge with temperature compensation.

Table 7: Sensor properties

Channel	Measured quantity	Sensor type	Sensitivity	Effective measuring range	Accuracy	Upper frequency limit
K1-K20	strain	RS L.11B.4	0.19 V^{-1}	0 ... 0.001	± 0.000005	∞
K22	pressure	QDE 100p	354 pC/MPa	0 ... 100 bar	± 1 bar	48 kHz
K23	pressure	QDE 20p	566 pC/MPa	0 ... 200 bar	± 2 bar	45 kHz
K24	pressure	QDE 100p	366 pC/MPa	0 ... 100 bar	± 1 bar	48 kHz
K25	pressure	QDE 20p	568 pC/MPa	0 ... 200 bar	± 2 bar	45 kHz
K26	pressure	QDE 20p	616 pC/MPa	0 ... 200 bar	± 2 bar	45 kHz
K27	pressure	QDE 20p	585 pC/MPa	0 ... 200 bar	± 2 bar	45 kHz

The measurements are stored in Excel® format. The test identifier is the date at which it was performed. This corresponds also to the name of the folder where the Excel files are stored. If more than one test was performed in a day the folder names are assembled from the date plus a consecutive letter (see column 1 of table 5). The names of the Excel files are assembled from the test date plus the channel numbers of the measurements which are stored in the file. Example: the file name "190601a_01,02,03.xls" means test no. 190601a (see table 5), channels 1, 2 and 3 (see table 6). The data files contain the measurement values and diagrams displaying the measuring quantities versus the time. The unit of the pressure signals is bar, the strains are dimensionless.

3.2.3 Selected results

All measurements are available as a set of Microsoft-Excel® files [6]. In this report the representative results are discussed based on selected data of different test series. Figures 10-21 show the measuring signals for the test no. 190601, figures 22-30 for the test no. 290601 and figure 31 shows the pressure signals measured in test no. 040701a. Figures 34-37 show a summary of all tests: the pressure amplitudes in dependence on the evacuation height $dH = H_1 - H_0$ (fig. 34), the pressure amplitudes in dependence on the evacuation pressure p_1 (fig. 35), the pressure amplitudes in dependence on the vessel pressure p_3 (fig. 36) and the pressure amplitudes in dependence on the valve opening time t_{open} (fig. 37).

The pressure signals consist of a part coming from the pressure wave (rectangular pulse with a length of about 5 ms) and a part coming from the stress wave in the pipe wall (overtone on the rectangular pulse), see figures 16,17,28,29. In the case of the fixed BP the pressure amplitude is a little bit higher than in the case of free BP, however, the shape of the signals are quite similar.

In the vertical pipe section in some distance from the bend the strains (and thereby the stresses) are more or less independent on the azimuthal position. That means in this part of the pipe there is no significant bending (fig. 10: MP1-D-0-T and MP1-D-180-T; fig. 12: MP3-D-0-T and MP3-D-180-T; fig. 22: MP1-D-0-T and MP1-D-180-T). The tangential strains in straight pipe section are correlated to the pressure signals (fig. 16), but they also contain some higher frequencies which most probably originate from the stress wave in the pipe wall. The sound velocity in the pipe wall is about 3 times higher than the sound velocity in the fluid. In the axial strain signals the shape of the pressure signals cannot be found, because the axial strain is mainly due to stress wave in the pipe wall.

In the pipe bend region the situation is more complicated. Axial and tangential strains are strongly coupled. Therefore the pressure wave and the stress wave can be seen in the both strain components. Moreover the low frequency global bending (excited by junction coupling) is also present in the strain signals. Figure 18 shows the pressure signal and the strain signals at the pipe bend intrados position for test no. 190601 (fixed bouncing plate). Figure 30 shows these signals for test no. 290601 with free bouncing plate. In this case the global bending vibration exhibits a significantly higher amplitude. The strain amplitudes due to global bending are even higher than those caused by the pressure wave itself. The frequency of the bending part in the strain signals is about 31 Hz. This corresponds to the second global in-plane bending mode of the filled CHWTF (see table 4).

The stress at the outer pipe wall side can be calculated from the according strain signals. Assuming a plane stress status the axial and the tangential stress components are:

$$\sigma_a = \frac{E}{1-\nu^2}\cdot[\varepsilon_a + \nu\varepsilon_t] \qquad \sigma_t = \frac{E}{1-\nu^2}\cdot[\varepsilon_t + \nu\varepsilon_a] \qquad \textbf{Eq. 4}$$

with $E = 2.0E{+}05$ MPa being the elasticity modulus of the pipe material and $\nu = 0.3$ the Poisson number. The figures 20, 21 show the stresses at MP3 and MP6 (extrados) for the test 190601 (fixed BP) and figures 32, 33 for test 290601 (free BP). In the case of fixed BP the maximum stress is about 60 MPa, in the case of free BP the maximum stress at the extrados position is about 130 MPa.

The influence of the evacuation pressure is demonstrated in figure 19. The maximum pressure amplitude is slightly decreased if the evacuation volume contains some residual air (p_1 = 40 mbar, p_1 = 50 mbar), see also figure 35. The pressure peaks occur at later times with increasing p_1 and the slope of the pressure increase becomes less steep (fig. 19).

Figure 31 shows the pressure signals of test no. 040701a with $p_1 = 0.029$ bar, $p_3 = 5$bar, $dH = 0.3$m, fixed BP. In this test the maximum pressure amplitude of $p = 106$ bar was reached. Because of the loosening of the fixation of the CWHTF only one shot could be performed, i.e. only the channels K22, K23, K24 were recorded.

Figure 38 shows two pressure signals of test no. 210901c. In this test the pressure sensor at MP1 (channel K22) was isolated, so it had no contact to the water. This pressure signals exhibits a very low amplitude compared to the not isolated sensor at MP2. This test demonstrates that the acceleration sensitivity of the pressure sensors is sufficiently low.

3.3 Summary of test results

The test results can be summarized as follows:

- in the straight pipe section the tangential strain signals correspond well with the pressure signals of the corresponding position
- the increase of the evacuation pressure leads to a decrease of the pressure slope and of the pressure amplitude
- the global bending of the CWHTF pipe system can be seen in the axial strain signals at the curvature; increasing evacuation pressure leads to decreasing strains
- if the valve opening time is increased to more than 0.5 s a significant reduction of the pressure amplitude occurs
- no influence of the acceleration on the pressure signal was measured

4 FSI-Modelling

The fluid-structure interaction occurring during a water hammer is characterized by two basic effects:

- The propagation of two coupled acoustic waves (the pressure wave in the fluid and the stress wave in the pipe wall)
- The common vibrations of fluid and pipeline which are governed by global dynamic properties of the pipe depending on geometry, boundary conditions, material, wall thickness etc. This is summarized under the term junction coupling.

The coupling of the fluid wave and the structural wave is based on the axial coupling at the bouncing location (point of origin of the waves) and on the radial coupling due the change of the pipe diameter. The axial strain of the pipe and the change of its diameter are connected via the cross contraction of the material (Poisson coupling).

The amplitude of the pressure wave can analytically be estimated by the extended Joukowsky formula:

$$\hat{p} = \frac{c_F \cdot \rho_F \cdot \Delta v}{\sqrt{1 + \frac{K_F}{E_P} \cdot \frac{D}{s}}} = c'_F \cdot \rho_F \cdot \Delta v \qquad \textbf{Eq. 5}$$

where the denominator represents the effect of the radial coupling between pipe and fluid displacement. However, this equation does not include the global dynamic behaviour of the pipe system (junction coupling).

After the initialisation of the water hammer the mean velocity of the fluid is zero. Thus it is not necessary to consider fluid flow effects. The finite element modelling can therefore be based on acoustic elements.

The pressure wave in a rigid pipe propagates with the sound velocity of the fluid. Thus, the travelling time in a pipe of the length L is given by L/c_F. In an elastic pipe the pressure wave travels with c'_F (cf. eq. 5). In a pipe with an open and a closed end the pressure signal at the closed end is a rectangular vibration with the basic period

$$T_0 = \frac{4 \cdot L}{c'_F} \qquad \textbf{Eq. 6}$$

In the case of the cold water hammer test facility with a pipe of $L = 3.280$ m, $D = 0.212$ m, $s = 6$ mm and the material parameters according to table 1, the time period is $T_0 = 10.5$ ms. The pressure peak according to eq. 5 (without consideration of junction coupling) amounts to $\hat{p} = 1.25$ MPa for a bouncing velocity of 1 m/s.

4.1 Finite element modelling

The finite element code ANSYS® is used for modelling. A 3D-model for cold water hammer test facility (CWHTF) of the FZR has been developed. The 3D-model comprises the vertical and the horizontal pipe section of the CWHTF including the bouncing plate [cf. fig. 39]. The vessel is not part of the model. The pipe wall is fixed at the corresponding position. The fluid pressure at that end is constant. The valve fixation is represented by spring elements. The model is shown in figures 39-42.

4.1.1 Coupling between fluid and structure

The FE-model consists of the pipe wall, which is meshed with structural SOLID45 elements, and the internal fluid, which is meshed with acoustic FLUID30 elements. The outer fluid surface and the inner pipe wall surface do not have common nodes. Instead of this there is a small gap between the fluid and the structure elements. This is necessary to enable a free slip in tangentional direction, i.e. parallel to the pipe axis. On the other hand the nodes of the fluid-structure interface are coupled in radial direction (i.e. normal to the fluid-structure interface). This is realized via the ANSYS command "CP".

The FLUID30 elements normally have only one degree of freedom (DOF), which is the pressure. If these elements are connected to structural elements (e.g. SOLID45), additional displacement DOFs (UX, UY, UZ) can be activated. To realize the displacement DOF activation it is necessary to cover the fluid elements (FLUID30) with a thin layer of structural elements SHELL43 (fig. 40). The shell elements and the outer surface of the fluid elements

have common nodes. The material properties of the shell elements are the same as the fluid element properties. It should be mentioned that the shell cover has no physical meaning, it is only necessary to activate the displacement DOFs of the FLUID30 elements. A direct connection between the fluid elements and the pipe wall elements is not possible, since it would prevent the free slip between pipe wall and fluid.

4.1.2 Simulation of the bouncing process

The simulation of the bouncing process consists of two short phases

- generation of the initial fluid velocity
- deceleration of the fluid front

The initial fluid velocity is generated by setting a displacement of the fluid front in a certain time interval t_0. Two load steps are used for this process. The transient effects are switched off to prevent the development of a dynamic pressure at that time. At the time t_0 the displacement of the whole fluid volume is u_0 and its velocity is v_{0F}, the dynamic pressure is zero.

In the deceleration phase the relative velocity between the fluid front and the bouncing plate is linearly decreased to zero within the time interval t_c (which represents the steam volume condensation time). In this phase the transient effects are switched on again. At the time $t = t_0 + t_c$ the displacement of the fluid front is zero and the velocity is equal to that of the bouncing plate v_c; the dynamic pressure is increased according to eq. 5. The deceleration of the fluid front is connected with an acceleration of the bouncing plate. Within the time interval $t_0 < t < t_0+t_c$ the bouncing plate velocity is linearly increased from zero to v_c. The time dependent fluid front motion is described by:

$$v_F(t) = v_{F0} - (v_{F0} - v_c)\cdot\frac{t-t_0}{t_c}$$

$$u_F(t) = u_{F0} + v_{F0}\cdot(t-t_0) - (v_{F0} - v_c)\cdot\frac{(t-t_0)^2}{2\cdot t_c} \qquad \textbf{Eq. 7}$$

$$u_F(t_0) = u_{F0} = u_c - \tfrac{1}{2}\cdot(v_{F0} + v_c)\cdot t_c$$

with u_c being the common displacement of fluid front and bouncing plate at $t=t_0+t_c$. The motion of the bouncing plate in the time interval $t_0 < t < t_0+t_c$ is described by:

$$v_B(t) = v_c\frac{t-t_0}{t_c}$$

$$u_B(t) = u_{B0} + v_c\cdot\frac{(t-t_0)^2}{2\cdot t_c} \qquad \textbf{Eq. 8}$$

$$u_{B0} = u_c - \frac{1}{2}\cdot v_c\cdot t_c$$

The velocity and displacement of bouncing plate and fluid front are shown in figure 43. The bouncing plate velocity at the end of the bouncing process, v_c, can be estimated from the balance between the pressure induced force and the inertia force of the bouncing plate (see fig. 44). Elastic forces coming from the pipe are neglected in that time frame.

$$p(t) \cdot A_F = m_B \cdot \ddot{u}_B(t)$$

$$A_F \cdot \int_{t_0}^{t_0+t_c} \hat{p} \left[\frac{t - t_0}{t_c} \right]^n dt = \frac{1}{n+1} \cdot A_F \cdot \hat{p} \cdot t_c = m_B \cdot v_c \qquad \textbf{Eq. 9}$$

The pressure is taken from the Joukowsky equation, which leads to:

$$v_c = \frac{v_{F0}}{1 + \frac{(n+1) \cdot m_B}{A_F c_F \rho_F t_c}} \qquad \textbf{Eq. 10}$$

At $t = t_0 + t_c$ the velocities of the bouncing plate and the fluid front are equal to v_c. At this time the contact between the fluid and the bouncing plate is locked. This is realized by activating extremely stiff beam elements. For $t < t_0 + t_c$ these coupling beams are deactivated (ANSYS commands "ekill" and "ealive").

4.1.3 Material properties

The pipe is made from the austenitic steel X4CrNi18-10 (DIN number 1.4301). A linear-elastic material behaviour is assumed in the FE-model. Table 8 shows the properties of the steel and water at room temperature.

Table 8: Material properties used in the FE model

Property	Steel 1.4301	Water
Elasticity modulus E [GPa]	200	-
Bulk modulus K [GPa]	167	2.1
Poisson ratio ν	0.3	0.5
Density ρ [kg/m³]	7850	997
Sound speed c [m/s]	5856	1450

The sound speed of water sensitively depends on the content of the air that is solved in the water. The value of $c_F = 1450$ m/s is valid for water at 25 °C without any solved air. In the FEM calculation this value is corrected.

4.2 Comparison of simulation and experiment

In [4] the experimental results of the CWHTF tests are documented. Table 5 shows the tests performed. In the FEM calculations the acceleration phase of the fluid (before bouncing) is not simulated. Therefore the test parameters evacuation height, valve opening time, evacuation pressure and gas vessel pressure, which were varied in the tests, cannot directly considered in the simulation. Instead the bouncing velocity can be varied in the FEM simulation. The fixation of the bouncing plate, which was also a test parameter, can be considered in the FEM simulation, too. Moreover the fixation of the valve [1] can be varied.

In view of this the following experiments are selected for comparison with FE simulation (Table 9):

Table 9: Tests selected for model validation					
Test name (as in Tab 4.1)	Fixation BP	Evacuation height [m]	Vessel pressure [bar]	Measured pressure peak [bar]	Estimated bouncing vel. [m/s]
290601	free	0.3	1	41	3.81
190601	fixed	0.3	1	44	3.81
020701	free	0.15	5	67	5.36

The total simulation time for all cases is 5.6 ms, which is a little bit more than the half period ($T_0/2$, eq. 6) of the expected pressure wave. Figure 2 shows the measurement positions at the CWHTF.

At first the comparison for the test case 290601 (table 9) is discussed. In figure 45 the experimental pressure at MP1 is compared with results of different simulations. The valve fixation and the initial velocity of the bouncing plate after bouncing are varied (eq. 9). It can be seen that the best agreement between simulation and test is achieved with a free valve and $v_c = 0.275 * v_{F0}$. Figures 46 and 47 show the comparison of measured and simulated pressures at MP1 and MP7. The agreement is good.

The simulation parameters were optimised as follows. The effective fluid sound velocity adjusted by the half wave period time ($T_0/2 = 0.0056$ s) to $c_{F,eff} = 0.8831 * c_F = 1311$ m/s; the steam volume condensation time was adjusted on the base of the slope of the measured pressure signals: $t_c = 0.5$ ms (cf. eq. 7 through 10); the parameter n=2 leads to an initial bouncing plate velocity of $v_c = 0.275 * v_{F0}$. The initial fluid velocity was calculated by an separated numerical model for the acceleration phase [1] and corrected on the base of the time difference between the trigger (valve opening) and the bouncing in the measurements (cf. figures 64 and 65).

Figure 48 shows a comparison of measured and simulated pressures and equivalent stresses. In spite of a good agreement of the pressure the stresses do not agree so well. The order of magnitude is right but the structures of the time signals are different. The reason for that could be a mistake in the application of the strain gauges (wrong glue).

Figures 54-57 show the pressure distribution at t = 0.6 ms, t = 1 ms, t = 1.5 ms and t = 2 ms respectively. It can be seen that the pressure wave travels through the pipeline starting at the bouncing plate. The figures 58-60 show the stress distribution in the pipe wall at the corresponding times (except 2 ms). The stress wave also starts at the bouncing plate, however, it travels faster than the pressure wave by a factor of about 4. This is a consequence of the different sound speeds of water and steel.

Figure 49 shows the fluid pressure over the time at different axial positions. It can be seen that the rectangular vibration of the period T_0 is superimposed by higher frequencies, which originate from the stress wave in the pipe wall. The positions MP1 ... MP7 correspond to the axial locations of the pressure sensors at the CWHTF [1-4]. The average pressure amplitude (plateau of the rectangular vibration without superimposed fluctuations) is about 4 MPa, which is less than predicted of by the extended Joukowsky equation (eq. 5). This is a consequence of the fact that the bouncing plate is not a rigid boundary but is accelerated during the bouncing process. (cf. chapter 4.1.2). Thus, the FE-model correctly describes the axial FSI. Figure 50 shows that the pressure in the bend does not differ much at the intrados and extrados position. Figures 51-52 show some stress signals over the time.

The results for the test case 190601 (table 9) are shown in the figures 61-63. Comparing figures 61 and 62 it can be seen that the simulation with a free bouncing plate meets the experiment better than the simulation with a fixed bouncing plate though the bouncing plate was fixed in the test. The conclusion is that a fixing of the bouncing plate (even it is relatively stiff) has almost no influence to the pressure wave amplitude. The bouncing plate fixation can only limit the secondary motion of the pipe (structural bending vibrations) which occurs later on as consequence of pressure hit. Within the time frame of about 10 ms after bouncing that is investigated here the fixation has almost no influence. This is also confirmed by the maximum measured pressure of the tests with and without fixation.

Figures 66-70 show the results of the test case 020701 (table 9). From the simulation's point of view this case is a simple scale up of the results of the test case 290601 since the pressure and stress signals are proportional to the bouncing velocity v_{F0}. However, in the experiment the pressure signals start with a flat slope, which leads to a time delay of the pressure peak (fig. 66). This is probably a consequence of some residual air in the evacuated volume. Besides the time shift of about 0.4 ms the time structures of the experimental pressure signal and the simulated pressure agrees very well. Again the agreement between the pressures is better than the agreement between the stresses (figure 67).

Figures 71-74 show the simulated pressure over time and the pressure distribution for different times in the case of a rigid pipe. It can be seen that the pressure wave travels without any disturbance through the pipe regardless of the change of direction caused by the pipe. It can be concluded that the scattered pressure distributions in the case of the elastic pipe (e.g. fig. 55) are not a consequence of wave reflections at the bend but that they are due to FSI.

5 Summary and assessment

The developed FE-model is capable of describing the FSI during a water hammer. It is validated based on experimental results from CWHTF tests. The model considers the following important phenomena:

- coupling of the fluid pressure wave and stress wave in the pipe wall (including junction coupling, Poisson coupling and axial coupling)
- non-axisymmetric stress and pressure distribution in the pipe bend (this is not possible with 1D algorithms, [7,8])
- bouncing plate acceleration during steam condensation

The model can describe as well the primary pipe wall motion (that is coupled to the pressure wave) as the secondary pipe motion (bending vibration after the water hammer). However, for the simulation of the secondary motion a 1D model (beam elements with internal fluid) would be sufficient and more efficient. Because of the high numerical effort the 3D FE-modelling of the FSI is the appropriate tool for the analysis of parts of pipe systems. Complex pipe systems have to analyzed by use of 1D algorithms. However, the 3D modelling is very useful to study local phenomena in the vicinity of bends, junctions or cones. Such local effects (which can not be investigated by 1D models) are:

- regions of stress concentrations in the pipe wall
- the radial and circumferential distribution of fluid pressure
- skewness and disaggregation of the pressure wave front caused by FSI

Therefore an improved evaluation of the mechanical integrity is possible in regions of interest of pipe systems. Usual commercial finite element codes like ANSYS can be used for the analysis of 3D FSI effects in pipes. The model should be assembled by acoustic (fluid) and structural elements (pipe). It is important to realize the coupling between fluid and structure elements in the right way. Some additional analytical effort is necessary to generate the initial velocity of the fluid and to describe the steam condensation phase during bouncing.

6 Acknowledgment

The experimental and theoretical work was done in the frame of the project "Two-Phase Flow Water Hammer Transients and Induced Loads on Materials and Structures of Nuclear Power Plants" (WAHALoads) –contract FIKS-CT-2000-00106 – sponsored by the European Community (5th framework programs).

7 References

[1] StarStruct® users manual Rev. 5.1; GenRad Inc., 1994

[2] Natke, H.-G.: Einführung in Theorie und Praxis der Zeitreihen- und Modalanalyse; Vieweg Verlag 1988

[3] Deliverable D22 of the WAHALoads-project: Description of the Cold Water Hammer Test Facility (CWHTF) at FZ-Rossendorf, March 2001

[4] Deliverable D23 of the WAHALoads-project: Experiment Specification Report for Stress Measurements at the CWHTF, March 2001

[5] Deliverable D24 of the WAHALoads-project: Quick Look Report for Stress Measurements at the CWHTF, October 2001

[6] Deliverable D26 of the WAHALoads-project: Measurement Data Set of the Tests Performed at the CWHTF, December 2001

[7] Deliverable D25 of the WAHALoads-project: Data Evaluation Report on Stress Measurements at CWHTF, December 2001

[8] Deliverable D27 of the WAHALoads-project: Fluid-Structure Interaction Modelling in the Finite Element Code ANSYS®, June 2002

Appendix: Figures

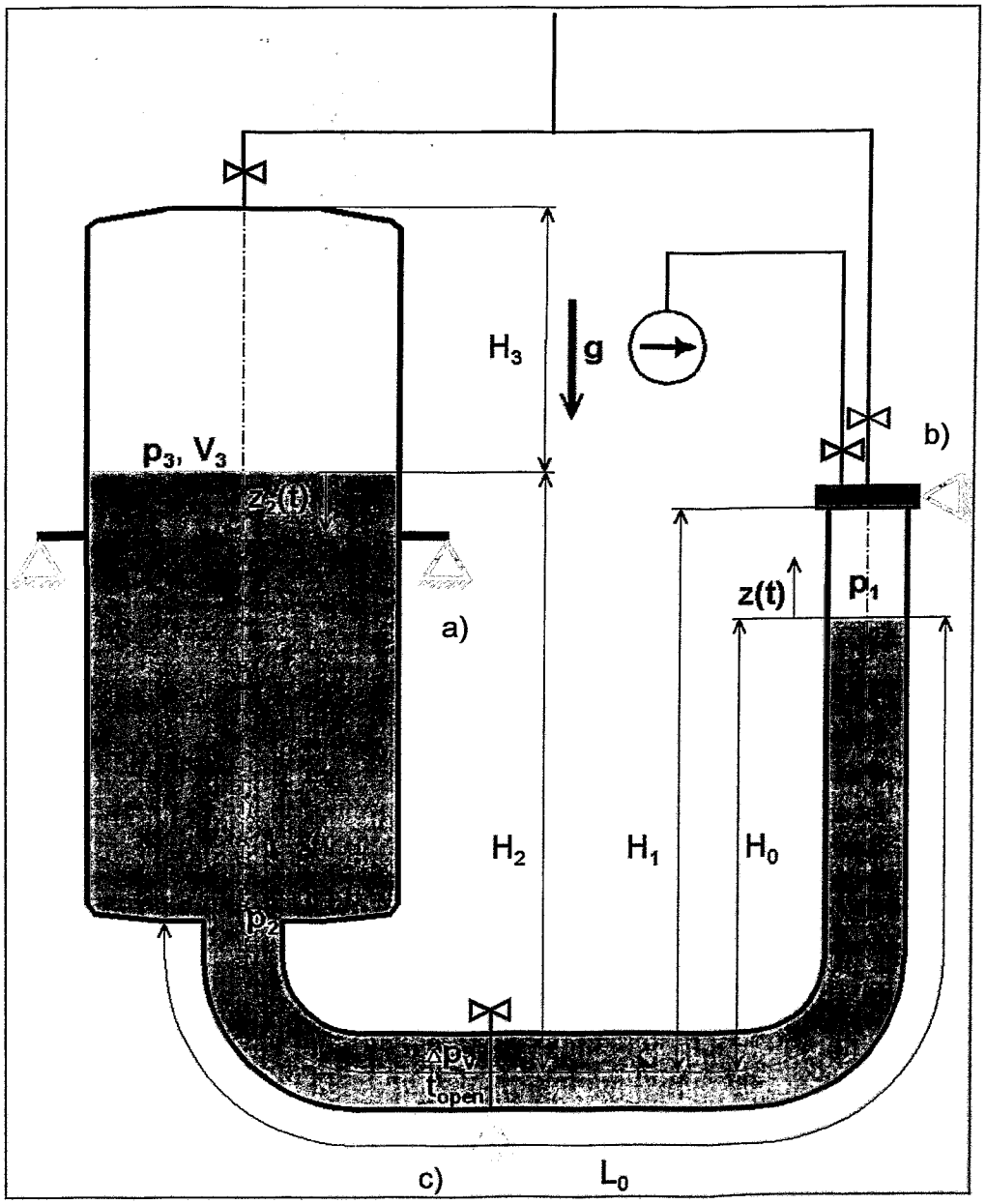

Figure 1: Main quantities of the CWHTF. Test parameter variations are made for: H_0, H_3, p_1, p_3, t_{open}. Furthermore the fixation of the bouncing plate will be varied; a) fixation vessel; b) fixation bouncing plate ; c) fixation valve

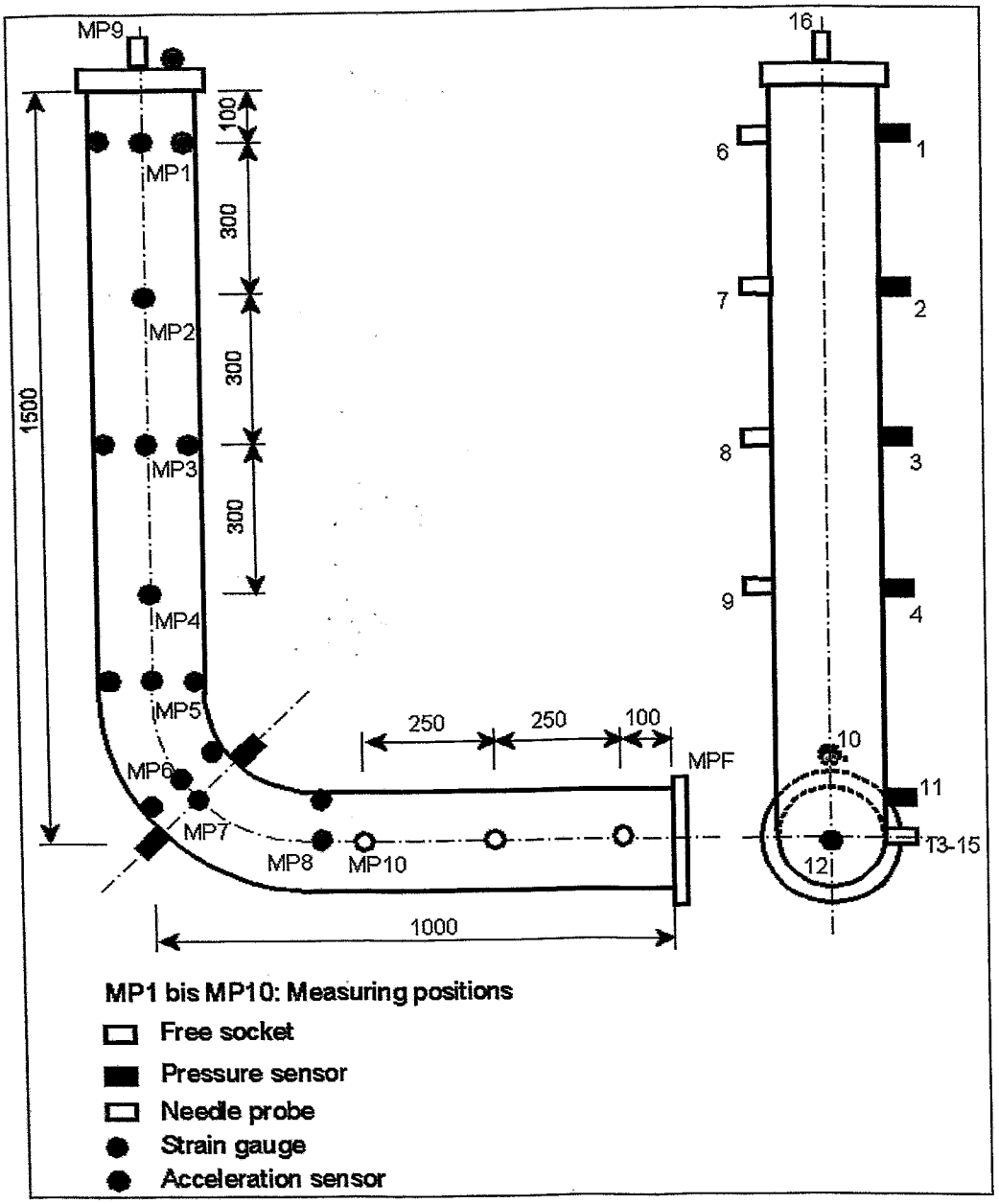

Figure 2: Instrumentation and measuring positions

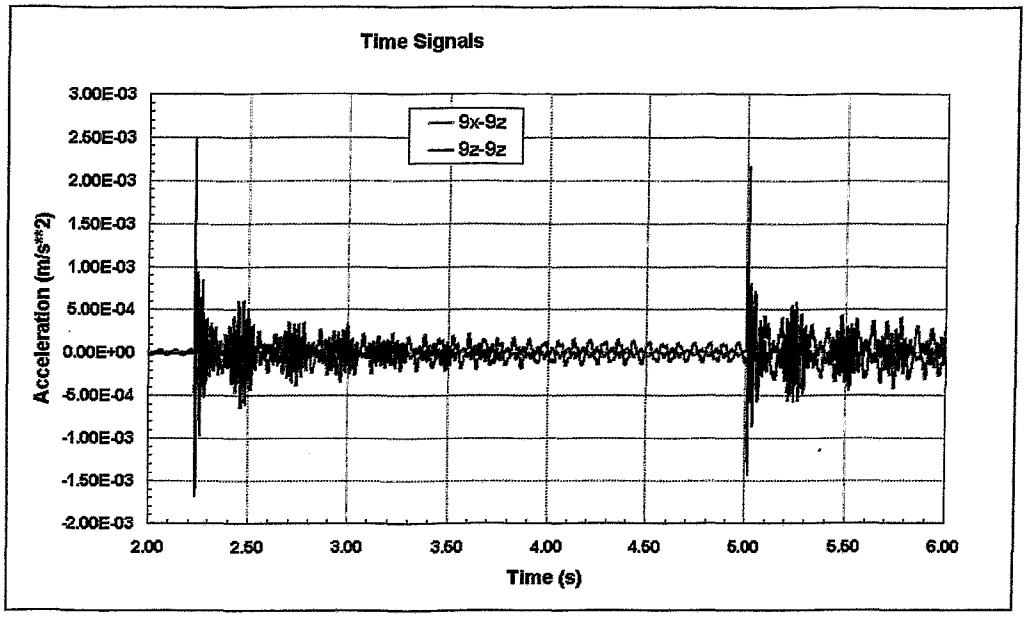

Figure 3: Acceleration signals from the modal analysis test at MP9; red: x-direction (horizontal in plane), blue: z-direction (vertical)

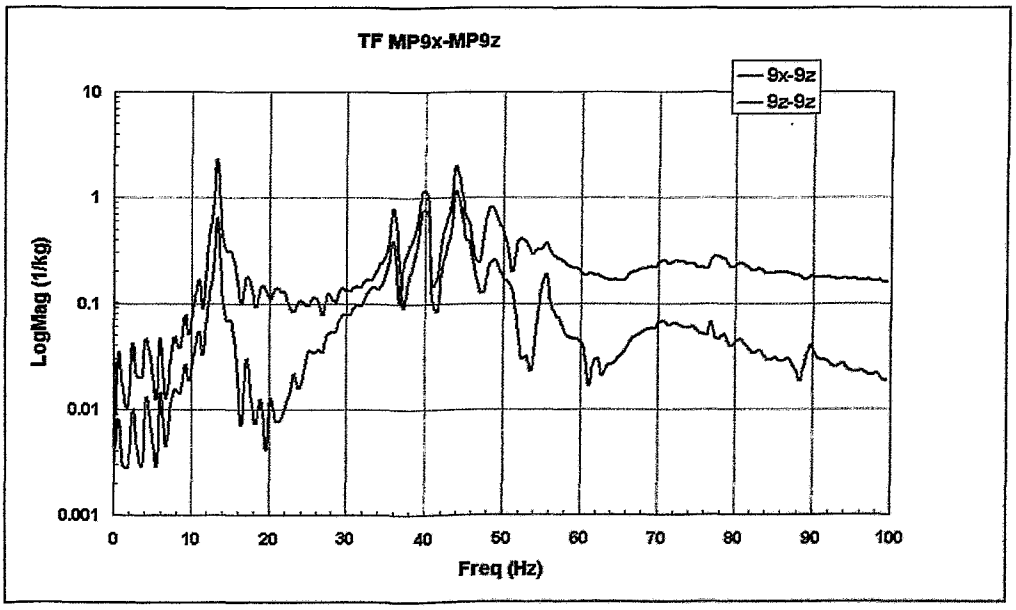

Figure 4: Transfer functions between accelerations at MP9 and impact excitation; red: x-direction (horizontal in-plane), blue: z-direction (vertical)

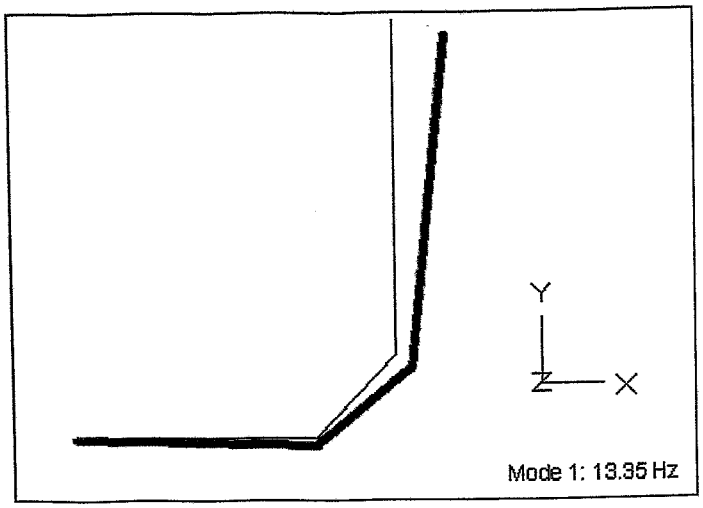

Figure 5: In-plane mode shape #1 of the empty CWHTF at 13 Hz

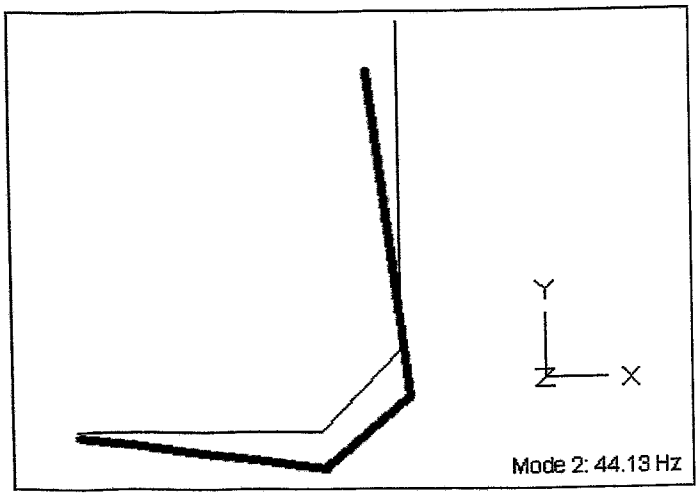

Figure 6: In-plane mode shape #2 of the empty CWHTF at 44 Hz

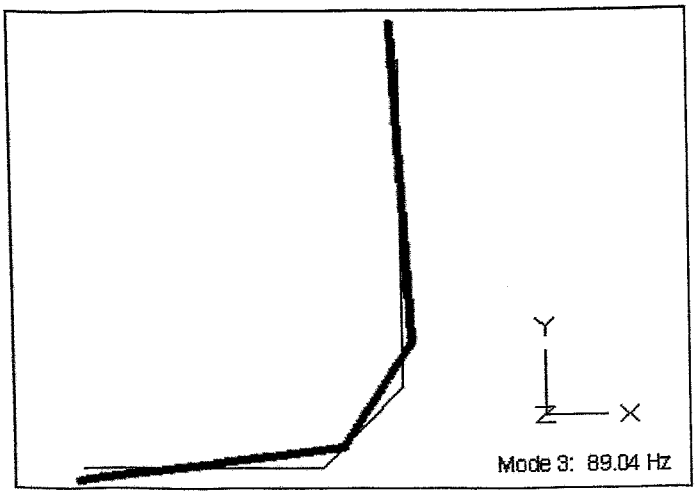

Figure 7: In-plane mode shape #3 of the empty CWHTF at 89 Hz

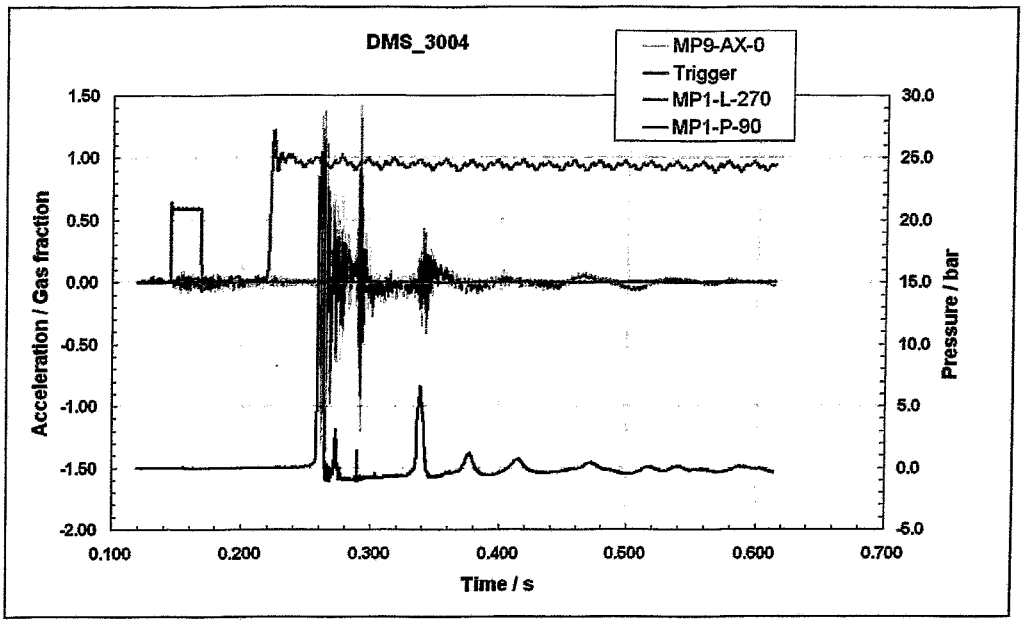

Figure 8: Black: pressure (bar) at MP1-90° (right ordinate axis); orange: horizontal (in-plane) acceleration [m/s²] of bouncing plate; blue: needle probe signal at MP1; green: trigger (valve opening phase); test with $v_0 = 3$ m/s, $t_{open} = 26.5$ ms, T = 20 °C, H_1-$H_0 = 0.155$ m, vessel closed.

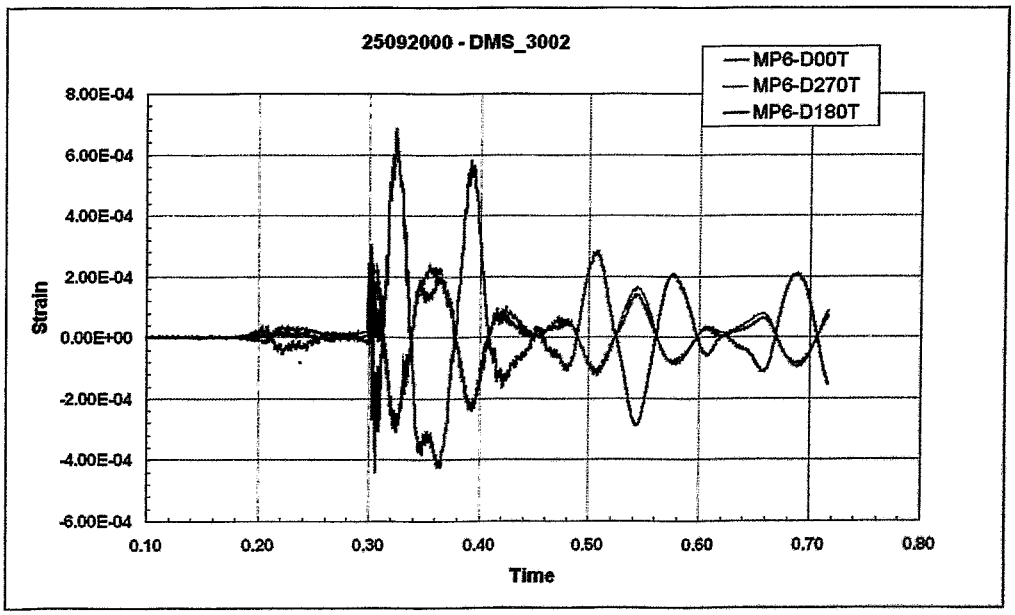

Figure 9: Tangential strains at MP6 (0°, 180°, 270°); pre-test with $v_0 = 3$ m/s, $t_{open} = 26.5$ ms, T = 20 °C, H_1-$H_0 = 0.155$ m

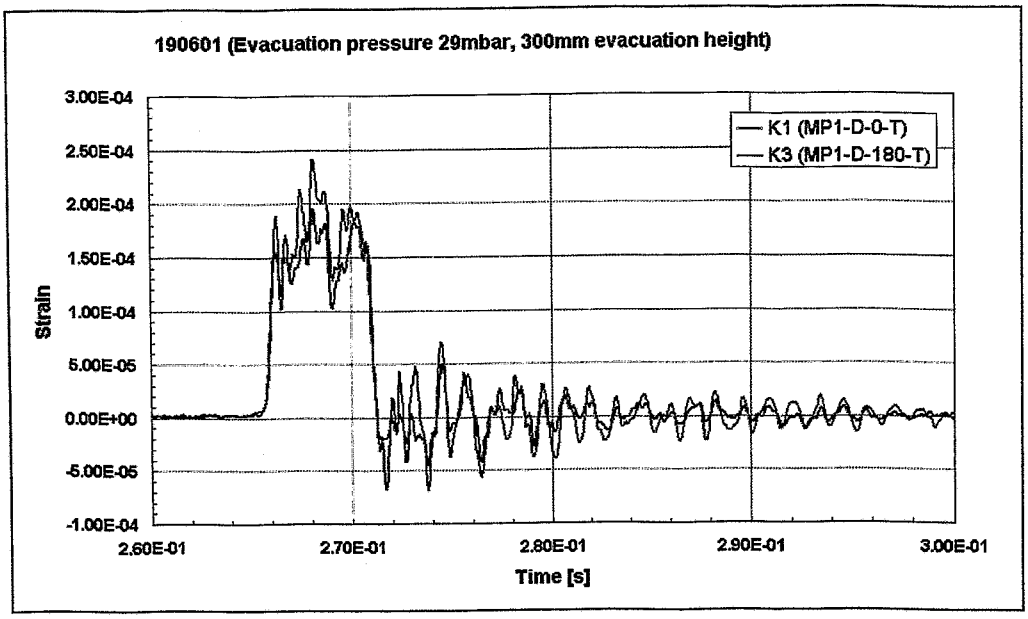

Figure 10: Tangential strain at MP1 0° and MP1 180°, axial strain at MP1 0°; test no. 190601: dH = 0.3 m, p_1 = 0.029 bar, p_3 = 1 bar, fixed BP

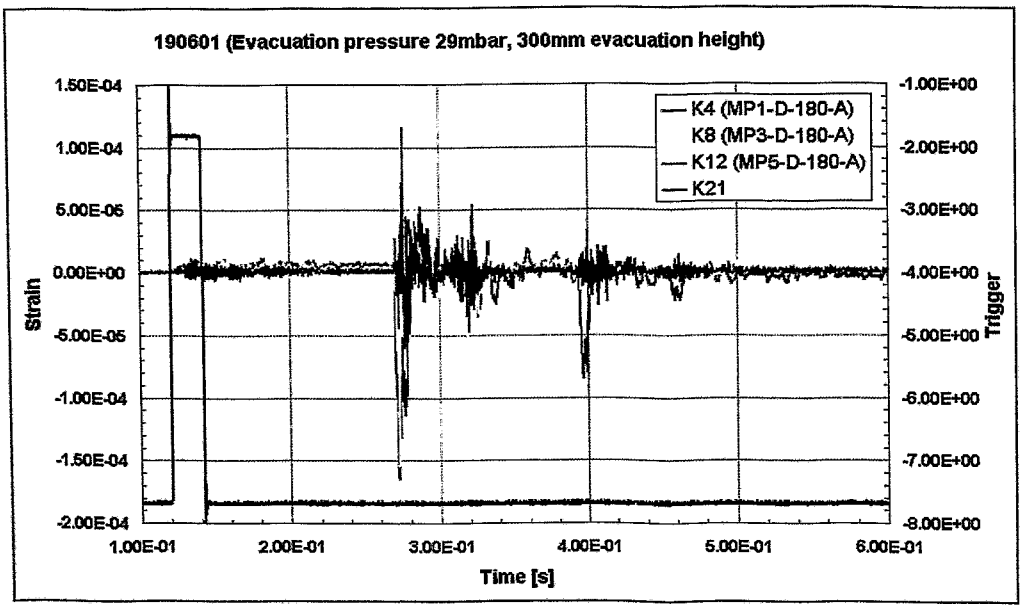

Figure 11: Axial strains at MP1 180°, MP3 180° and MP5 180°, trigger (valve opening); test no. 190601: dH = 0.3 m, p_1 = 0.029 bar, p_3 = 1 bar, fixed BP

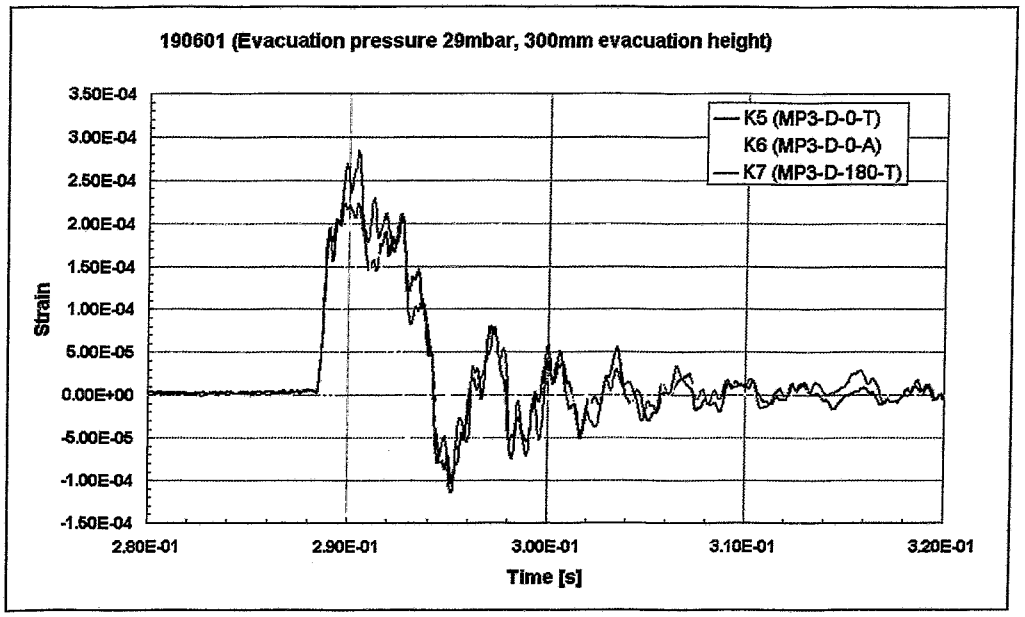

Figure 12: Tangential strain at MP3 0° and MP3 180°, axial strain at MP3 0°; test no. 190601: dH = 0.3 m, p_1 = 0.029 bar, p_3 = 1 bar, fixed BP

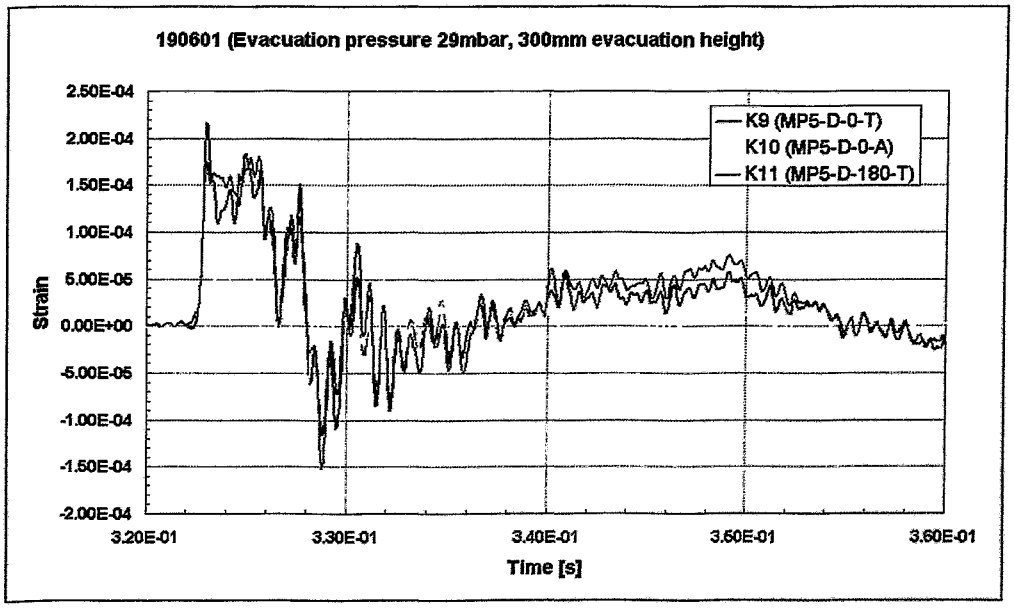

Figure 13: Tangential strain at MP5 0° and MP5 180°, axial strain at MP5 0°; test no. 190601: dH = 0.3 m, p_1 = 0.029 bar, p_3 = 1 bar, fixed BP

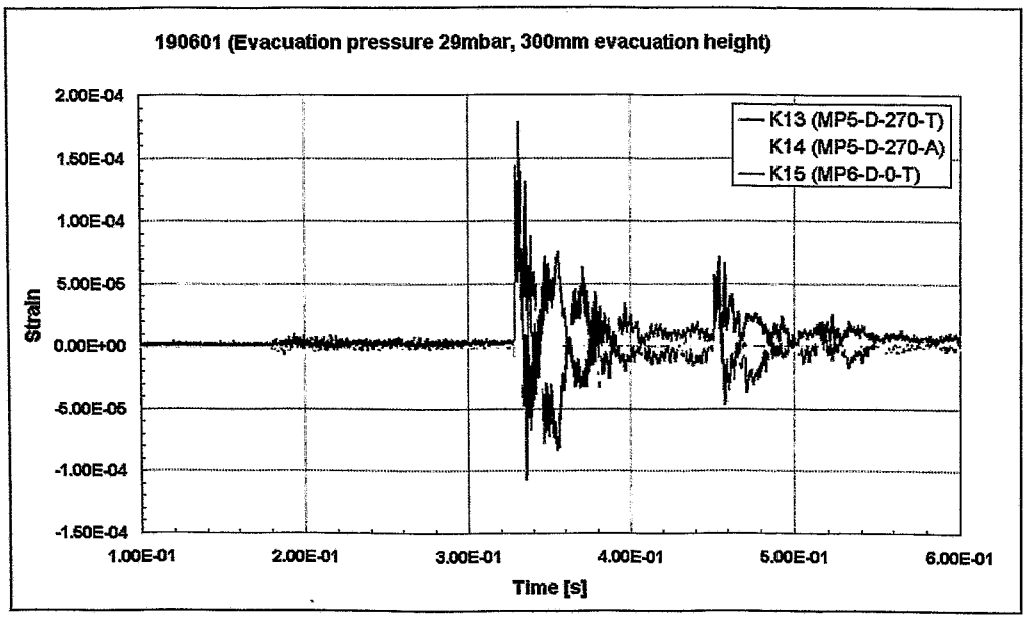

Figure 14: Tangential strain at MP5 270° and MP6 0°, axial strain at MP5 270°; test no. 190601: dH = 0.3 m, p_1 = 0.029 bar, p_3 = 1 bar, fixed BP

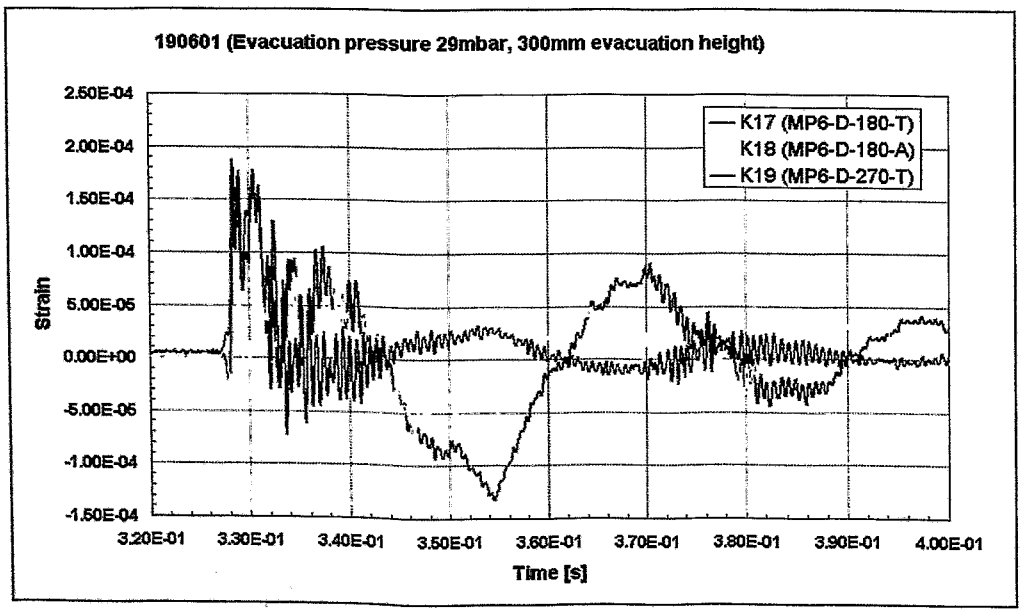

Figure 15: Tangential strain at MP6 180° and MP6 270°, axial strain at MP6 180°; test no. 190601: dH = 0.3 m, p_1 = 0.029 bar, p_3 = 1 bar, fixed BP

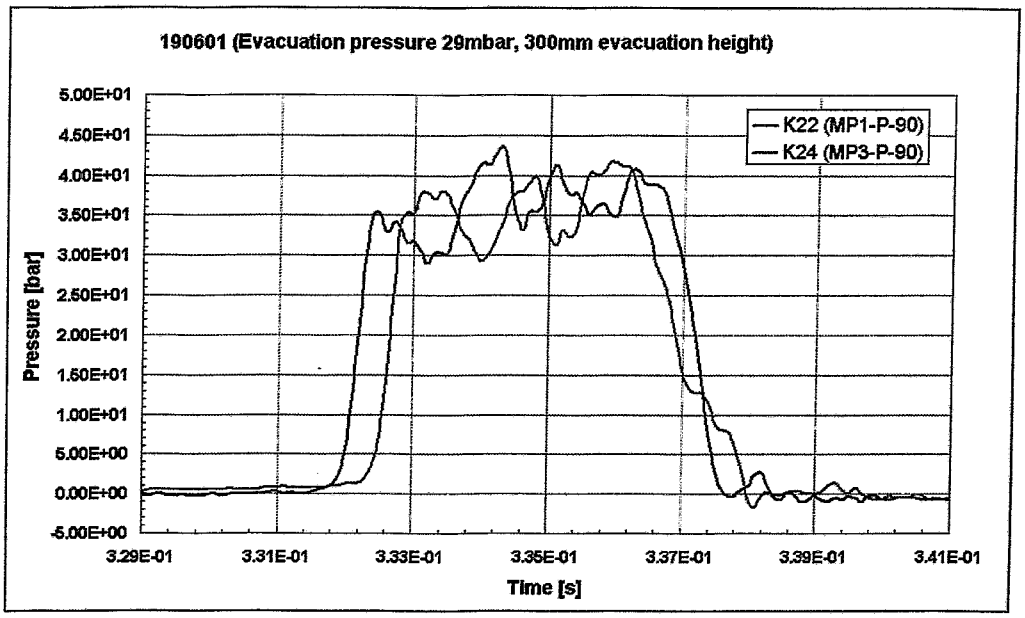

Figure 16: Pressure at MP1 90° and MP3 90°; test no. 190601: dH = 0.3 m, p_1 = 0.029 bar, p_3 = 1 bar, fixed BP

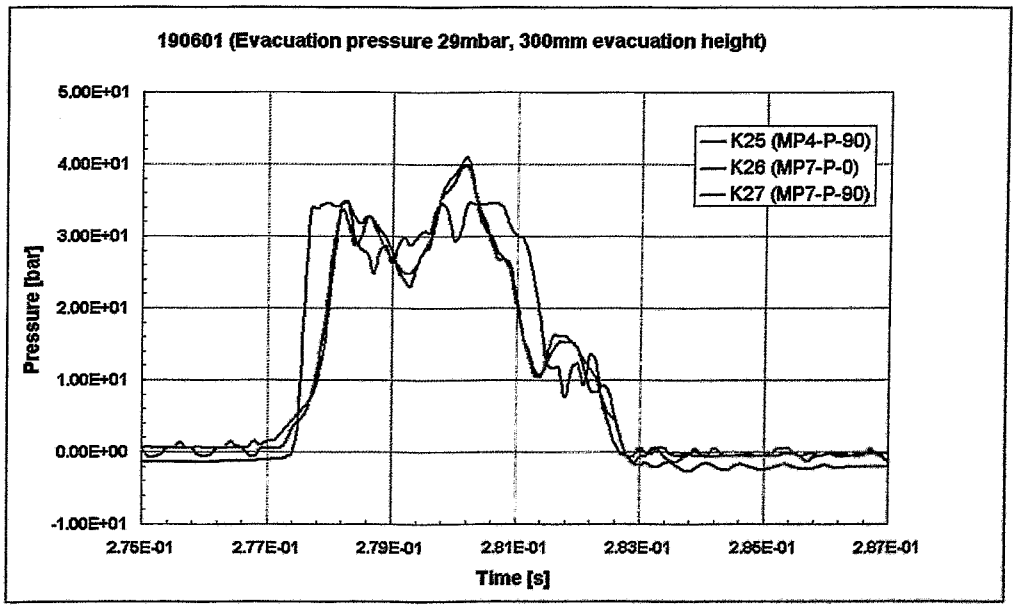

Figure 17: Pressure at MP4 90°, MP7 0° and MP7 90°; test no. 190601: dH = 0.3 m, p_1 = 0.029 bar, p_3 = 1 bar, fixed BP

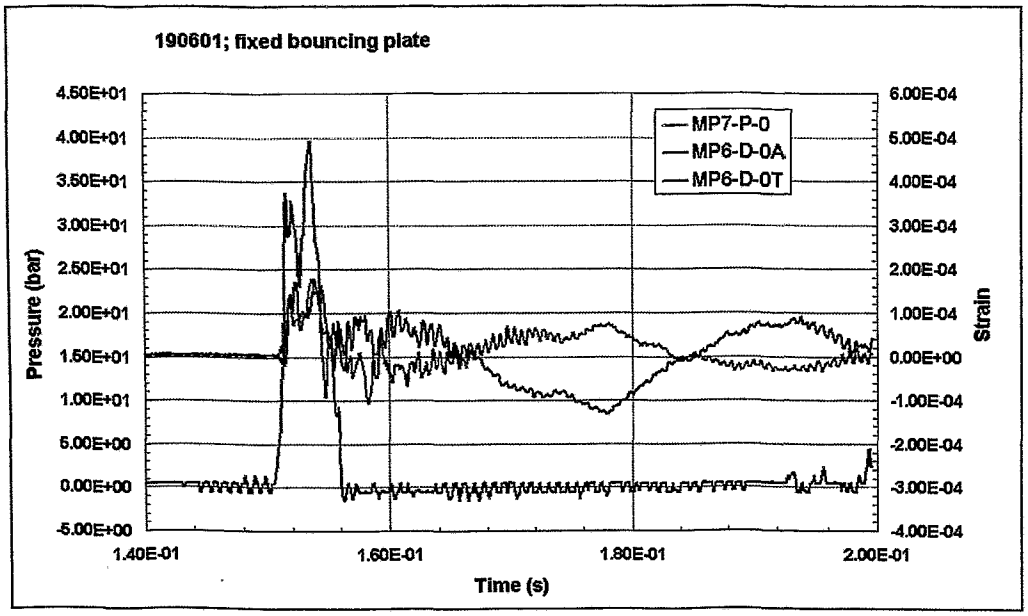

Figure 18: Pressure at MP7 0°, axial and tangential strain at MP6 0° (pipe bend intrados); test no. 190601: dH = 0.3 m, p_1 = 0.029 bar, p_3 = 1 bar, fixed BP

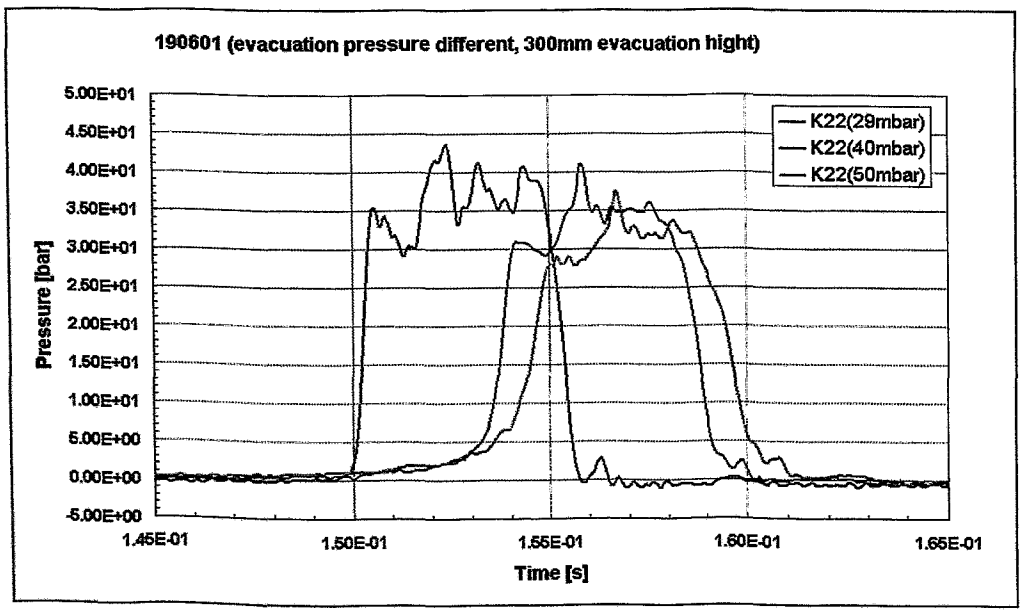

Figure 19: Pressure at MP1 90° for different evacuation pressures p_1; test 190601 (p_1 = 29 mbar), test 190601a (p_1 = 40 mbar), test 190601b (p_1 = 50 mbar); pressure signals are synchronized with trigger signals

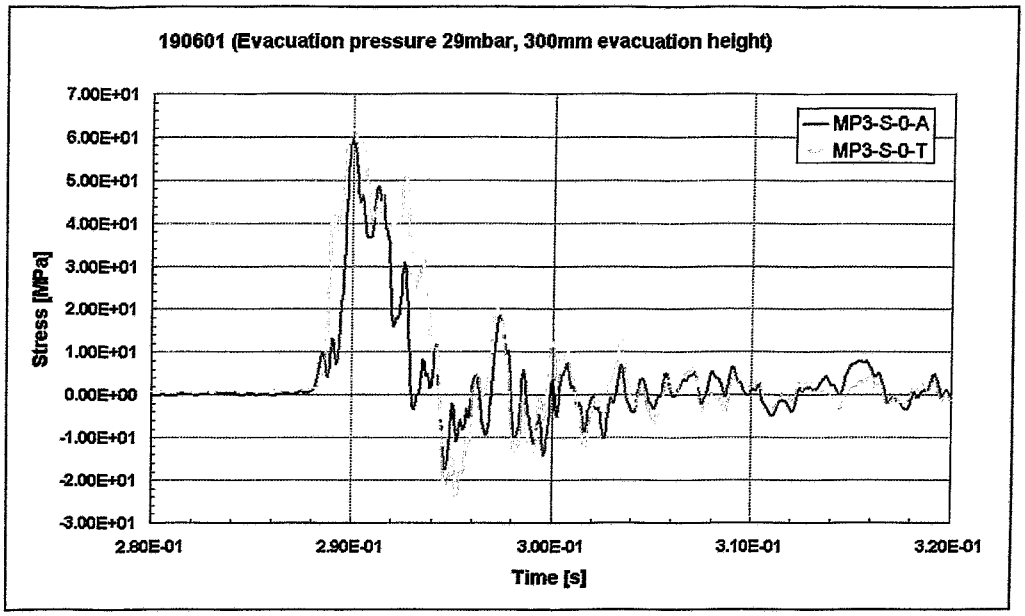

Figure 20: Axial and tangential stress at MP3 0° (calculated from the strain signals); test no. 190601: dH = 0.3 m, p_1 = 0.029 bar, p_3 = 1 bar, fixed BP

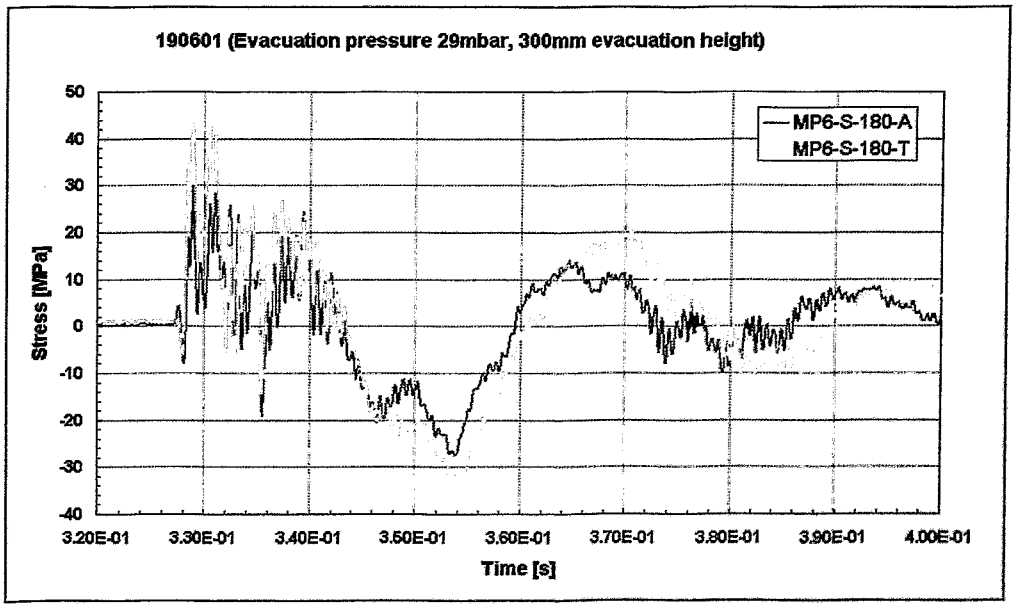

Figure 21: Axial and tangential stress at MP6 180° (calculated from the strain signals); test no. 190601: dH = 0.3 m, p_1 = 0.029 bar, p_3 = 1 bar, fixed BP

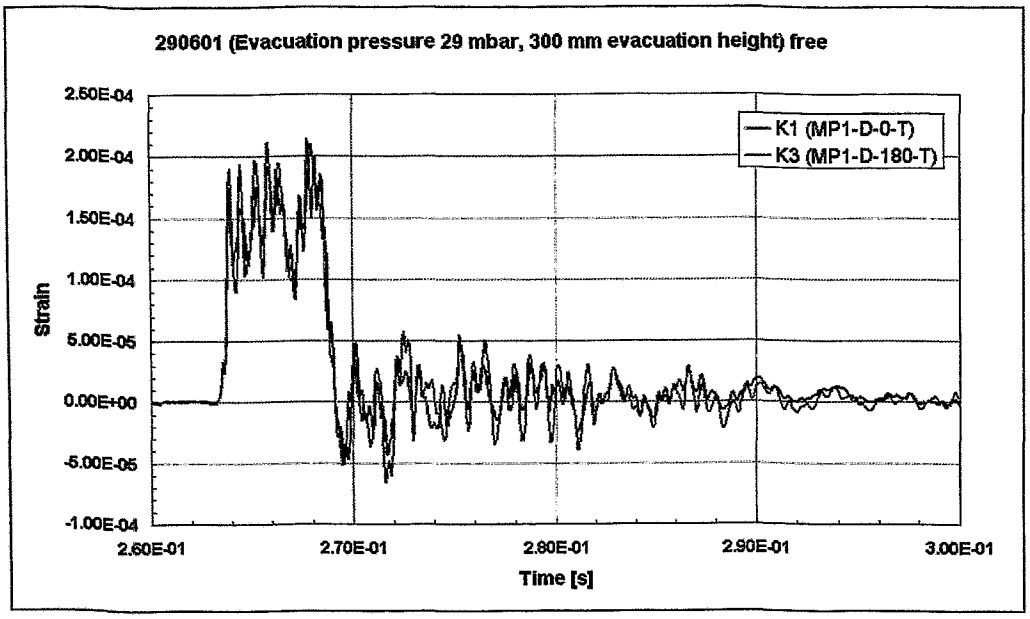

Figure 22: Tangential strain at MP1 0° and MP1 180°; test no. 290601: dH = 0.3 m, p_1 = 0.029 bar, p_3 = 1 bar, free BP

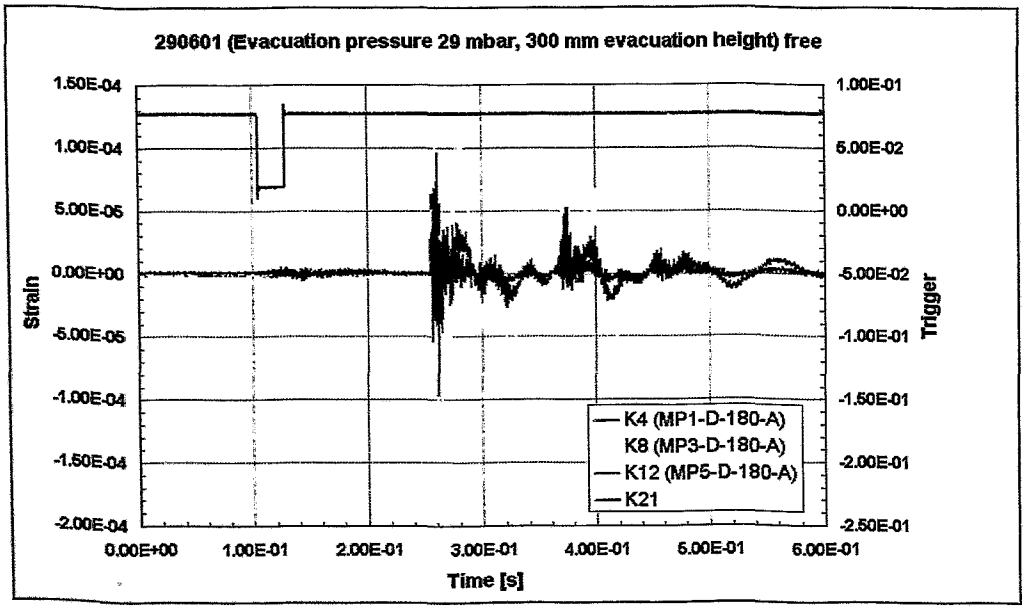

Figure 23: Tangential strain at MP1 180°, MP3 180° and MP5 180°, trigger (valve openeing); test no. 290601: dH = 0.3 m, p_1 = 0.029 bar, p_3 = 1 bar, free BP

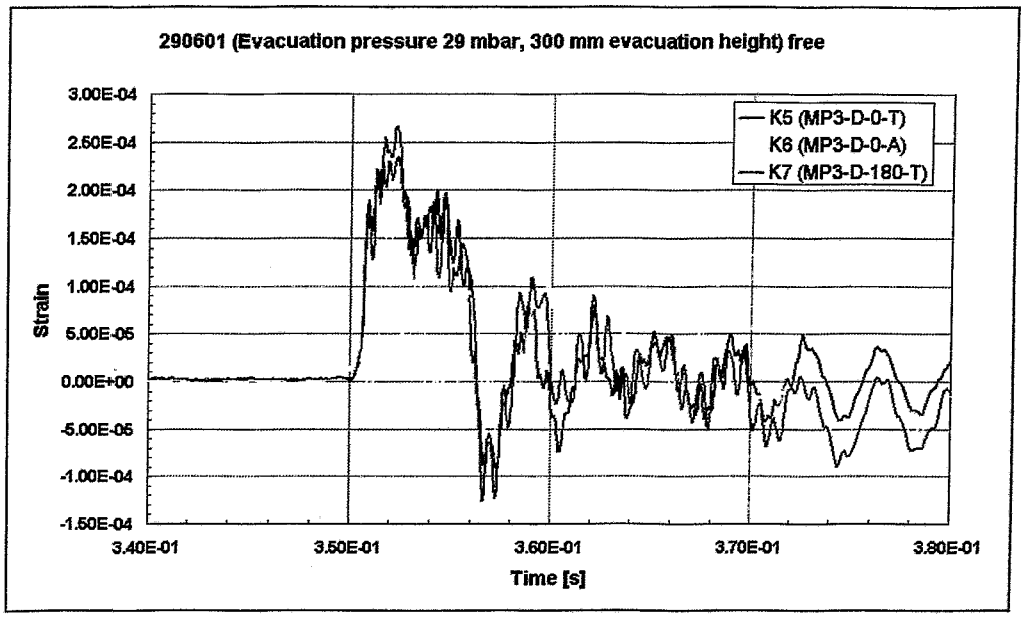

Figure 24: Tangential strain at MP3 0° and MP3 180°, axial strain at MP3 0°; test no. 290601: dH = 0.3 m, p_1 = 0.029 bar, p_3 = 1 bar, free BP

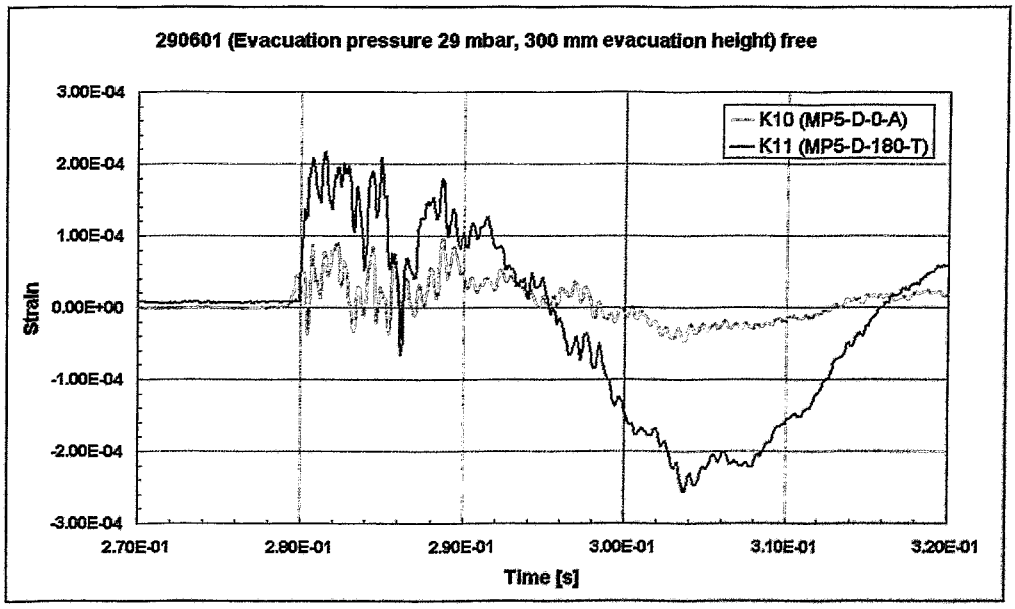

Figure 25: Tangential strain at MP5 180° and axial strain at MP5 0°; test no. 290601: dH = 0.3 m, p_1 = 0.029 bar, p_3 = 1 bar, free BP

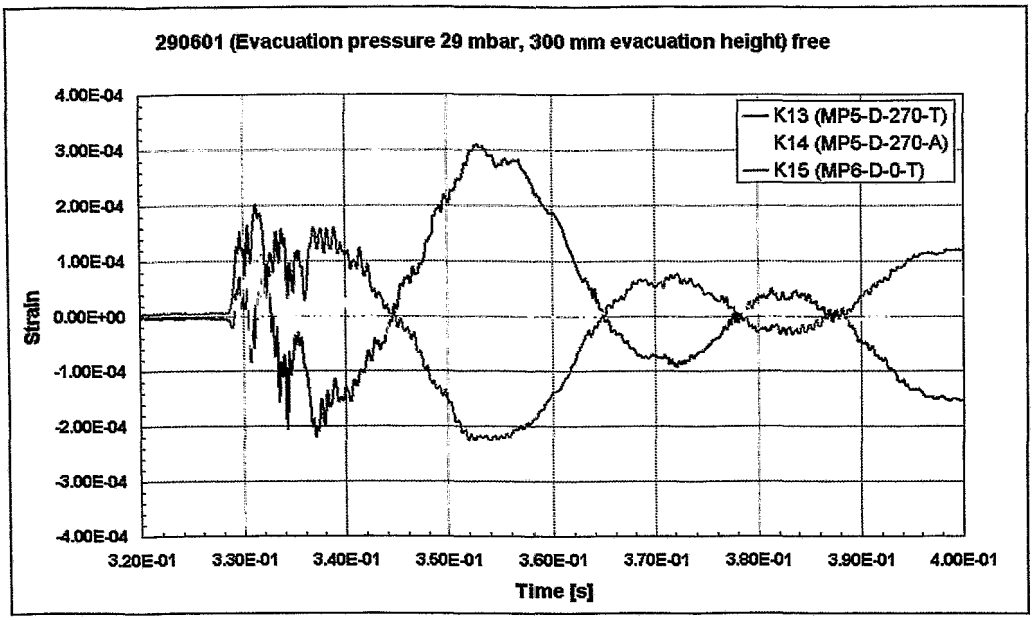

Figure 26: Tangential strain at MP5 270° and MP6 0°, axial strain at MP5 270°; test no. 290601: dH = 0.3 m, p_1 = 0.029 bar, p_3 = 1 bar, free BP

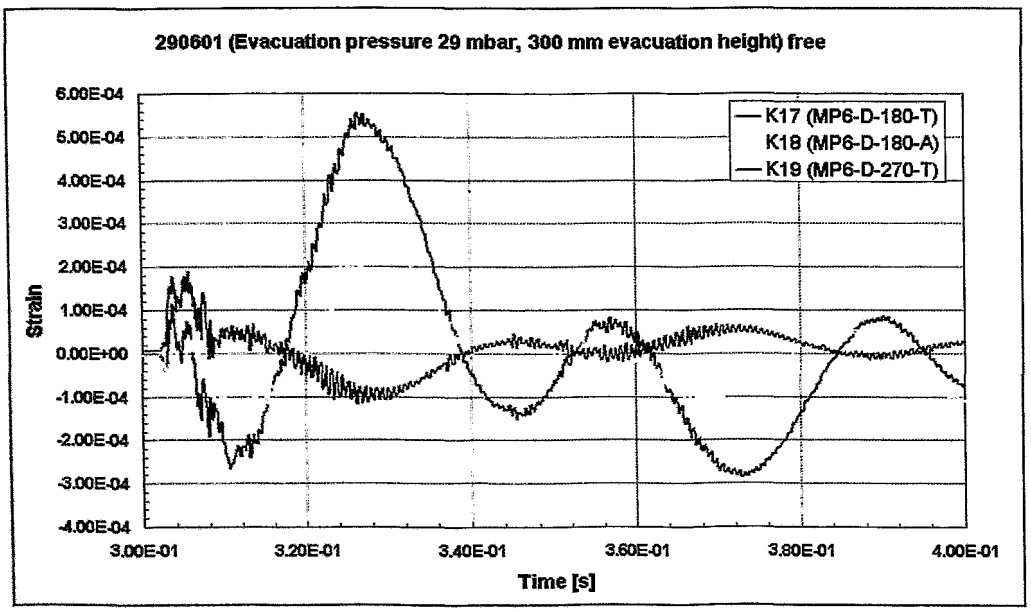

Figure 27: Tangential strain at MP6 180° and MP6 270°, axial strain at MP6 180°; test no. 290601: dH = 0.3 m, p_1 = 0.029 bar, p_3 = 1 bar, free BP

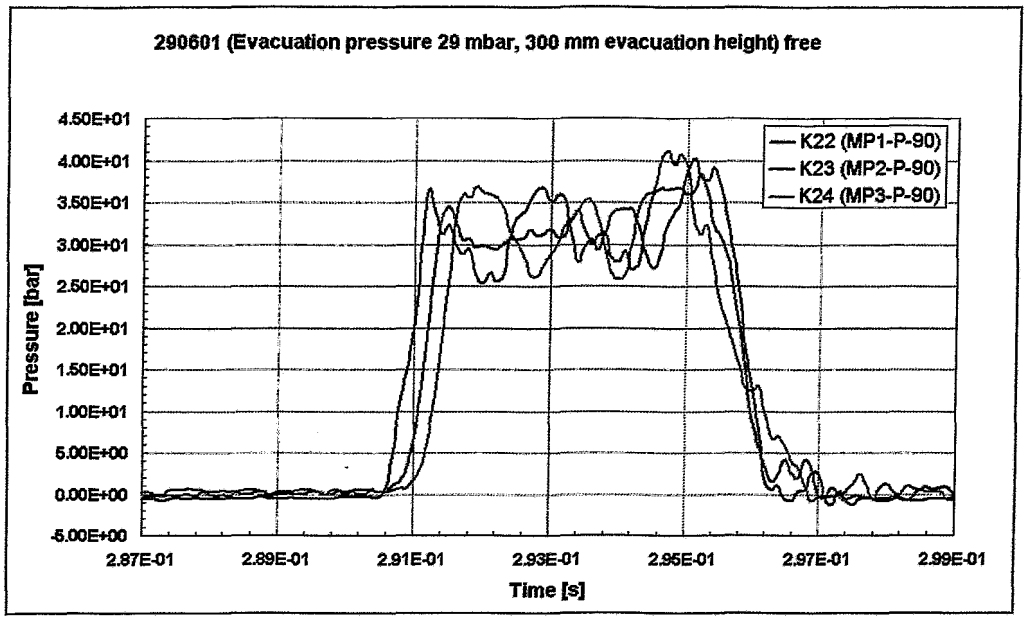

Figure 28: Pressure at MP1 90°, MP2 90° and MP3 90°; test no. 290601: dH = 0.3 m, p_1 = 0.029 bar, p_3 = 1 bar, free BP

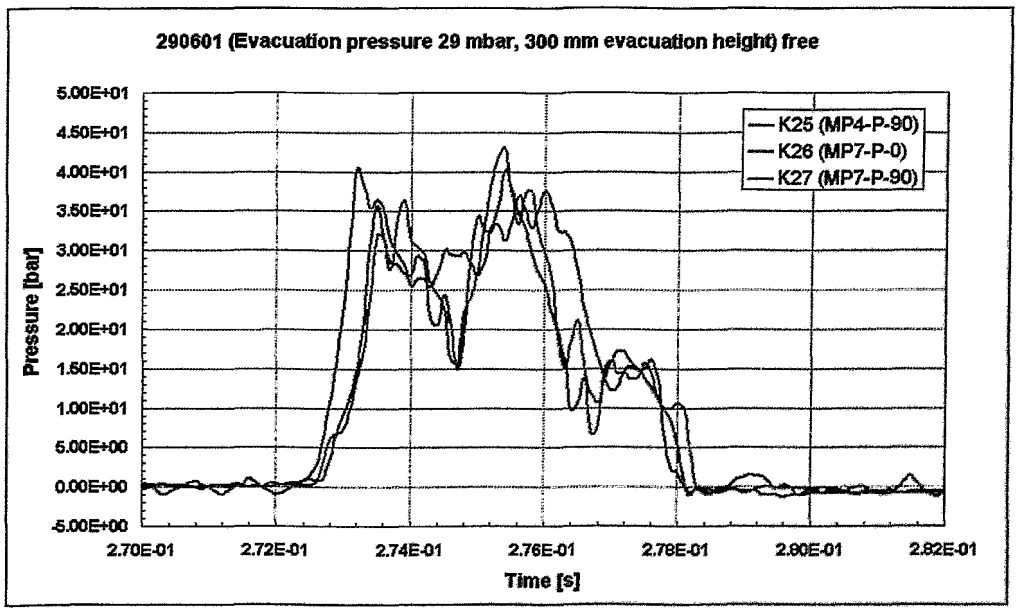

Figure 29: Pressure at MP4 90°, MP7 0° and MP7 90°; test no. 290601: dH = 0.3 m, p_1 = 0.029 bar, p_3 = 1 bar, free BP

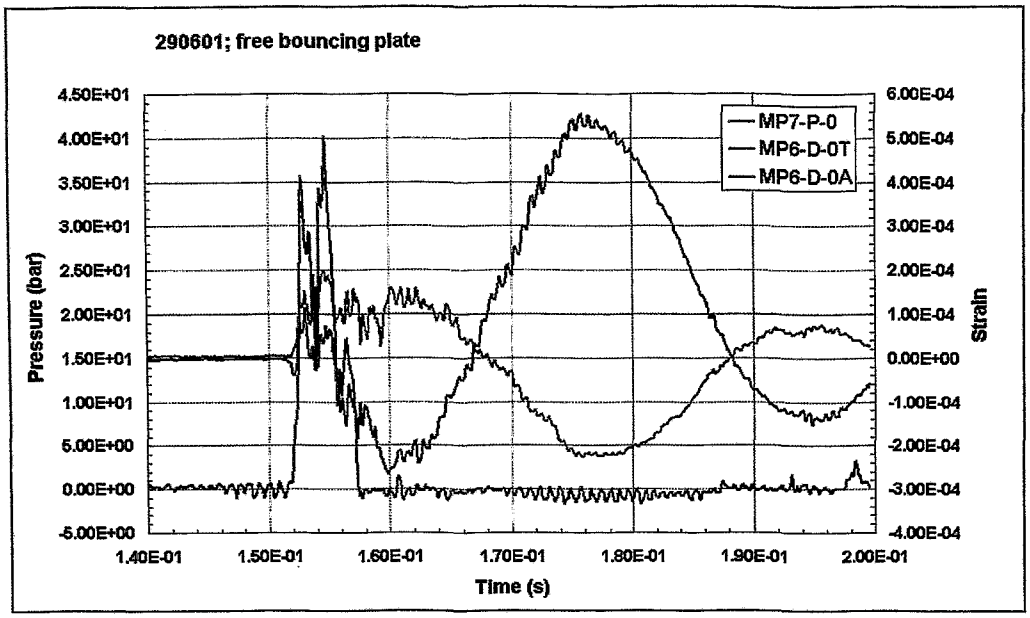

Figure 30: Pressure at MP7 0°, axial and tangential strain at MP6 0° (pipe bend intrados); test no. 290601: dH = 0.3 m, p_1 = 0.029 bar, p_3 = 1 bar, free BP

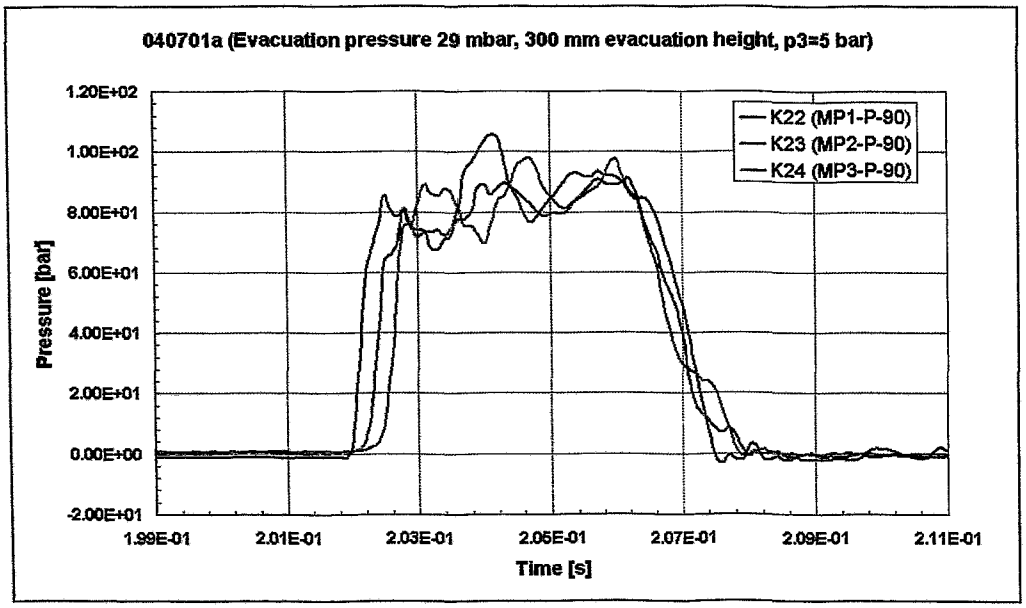

Figure 31: Pressure at MP1 90°, MP2 90° and MP3 90°; test no. 040701a: dH = 0.3 m, p_1 = 0.029 bar, p_3 = 5 bar, fixed BP

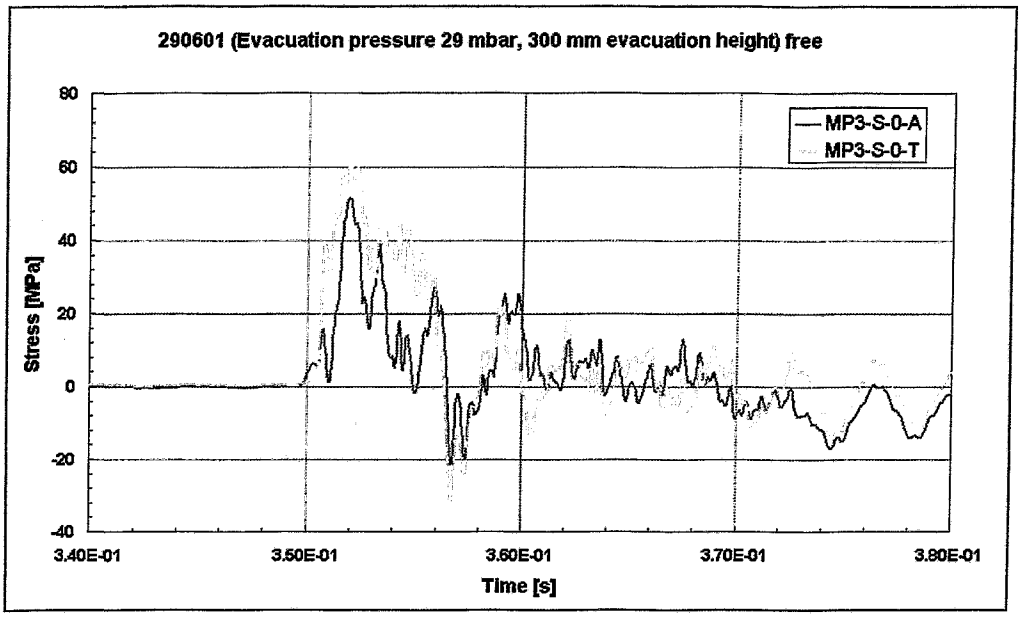

Figure 32: Axial and tangential stress at MP3 0° (calculated from the strain signals); test no. 290601: dH = 0.3 m, p_1 = 0.029 bar, p_3 = 1 bar, free BP

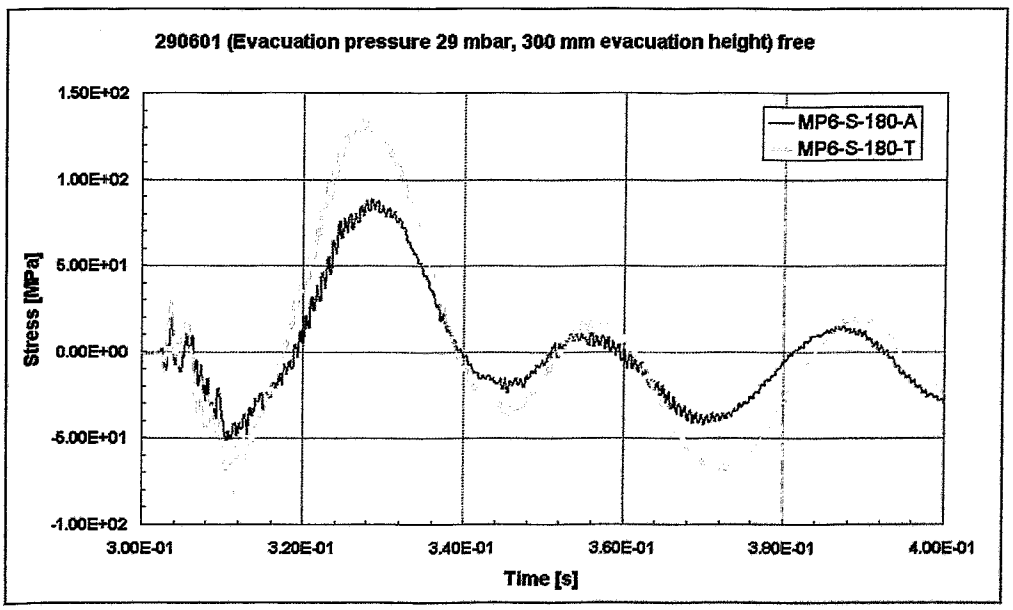

Figure 33: Axial and tangential stress at MP6 180° (calculated from the strain signals); test no. 290601: dH = 0.3 m, p_1 = 0.029 bar, p_3 = 1 bar, free BP

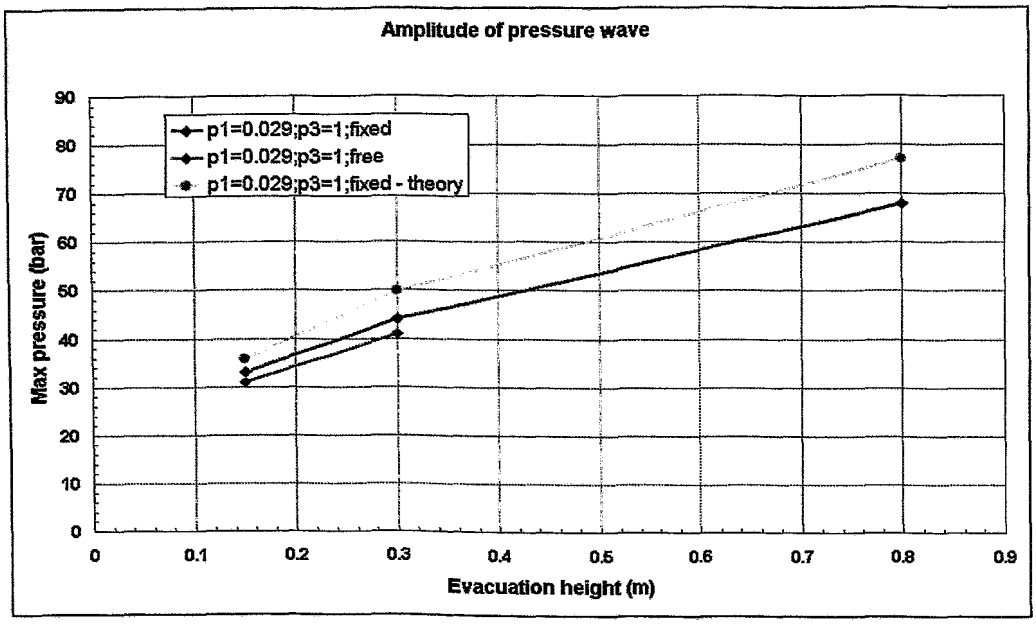

Figure 34: Pressure amplitude in dependence on evacuation height $dH=H_1-H_0$, blue: tests with $p_1 = 0.029$ bar, $p_3 = 1$ bar, fixed BP; orange: theory (1D-model) with $p_1 = 0.029$ bar, $p_3 = 1$bar, fixed BP; magenta: tests with $p_1 = 0.029$ bar, $p_3 = 1$bar, free BP

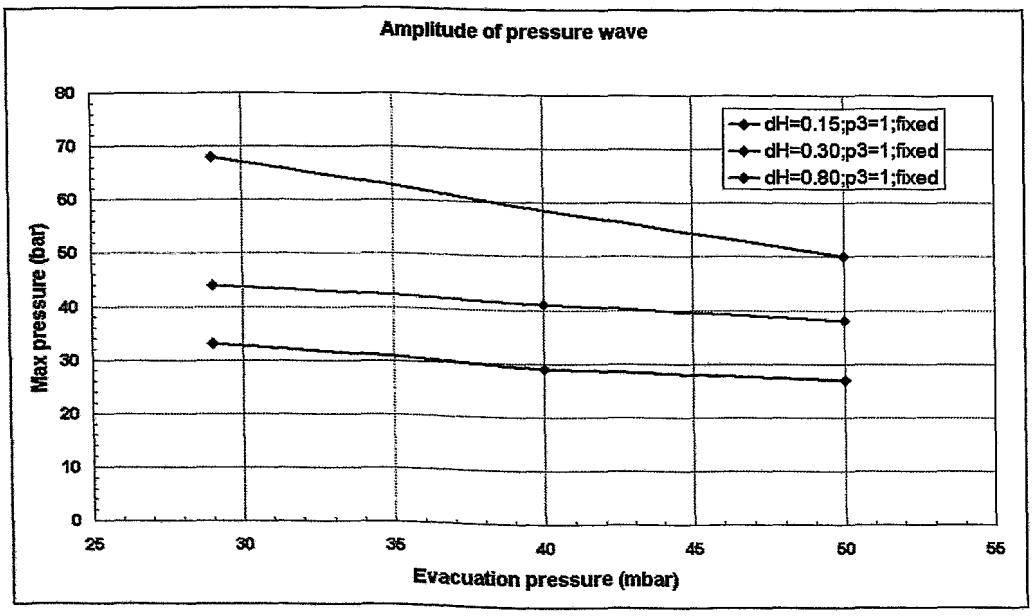

Figure 35: Pressure amplitude in dependence on evacuation pressure p_1, blue: tests with $dH = 0.15$ m, $p_3 = 1$ bar, fixed BP; magenta: tests with $dH = 0.30$ m, $p_3 = 1$bar, fixed BP; red: tests with $dH = 0.80$ m, $p_3 = 1$ bar, fixed BP

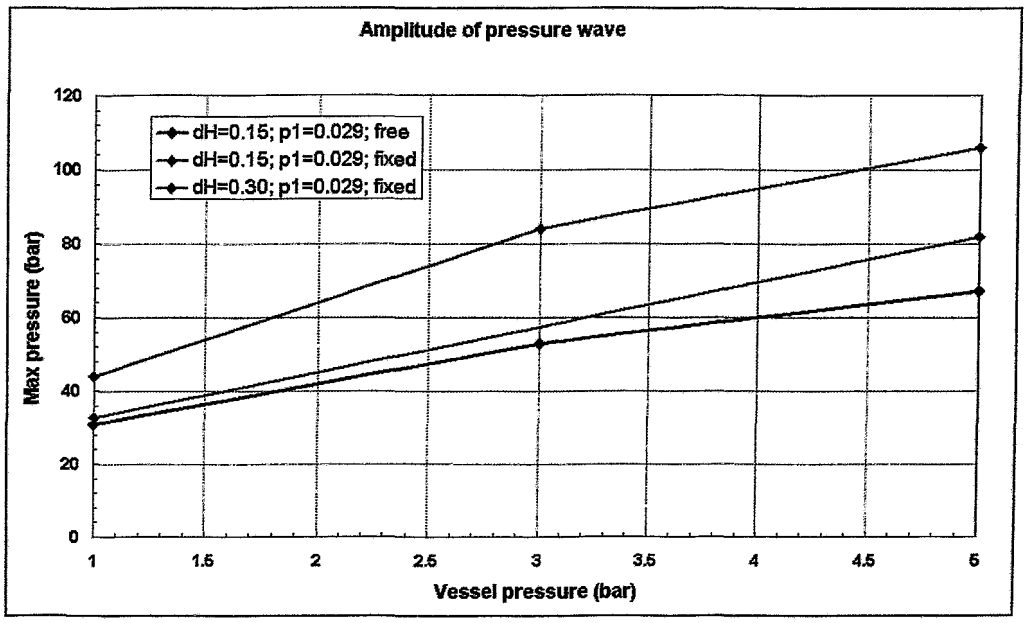

Figure 36: Pressure amplitude in dependence on vessel pressure p_3, blue: tests with dH = 0.15 m, p_1 = 0.029 bar, free BP; light blue: tests with dH = 0.15 m, p_1 = 0.029 bar, fixed BP; magenta: tests with dH = 0.30 m, p_1 = 0.029 bar, fixed BP

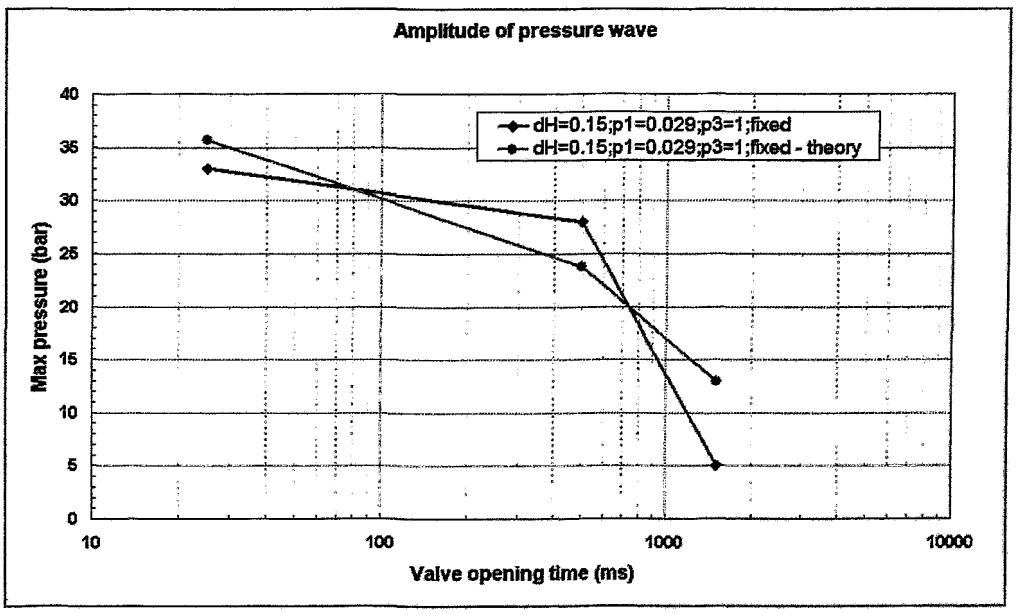

Figure 37: Pressure amplitude in dependence on valve opening time t_{open}, blue: tests with p_1 = 0.029 bar, p_3 = 1 bar, dH = 0.15 m, fixed BP; magenta: theory (1D-model) with p_1 = 0.029 bar, p_3 = 1 bar, dH = 0.15 m, fixed BP

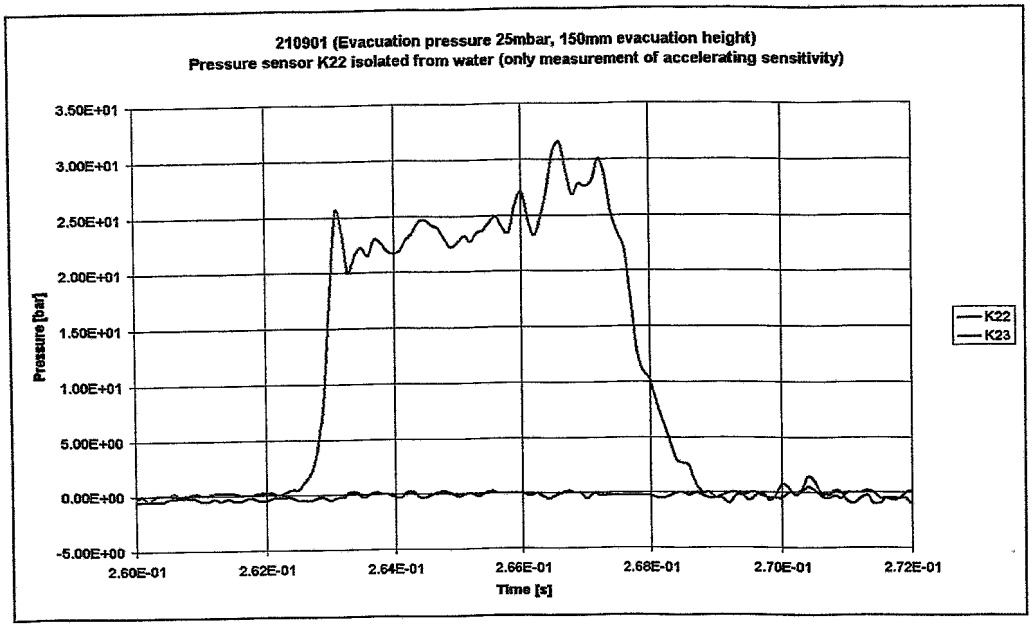

Figure 38: Pressure at MP1 90° and MP2 90°; test no. 210901c: dH = 0.15 m, p_1 = 0.029 bar, p_3 = 1 bar, fixed BP; nozzle of MP1-P-90 (K22) was isolated

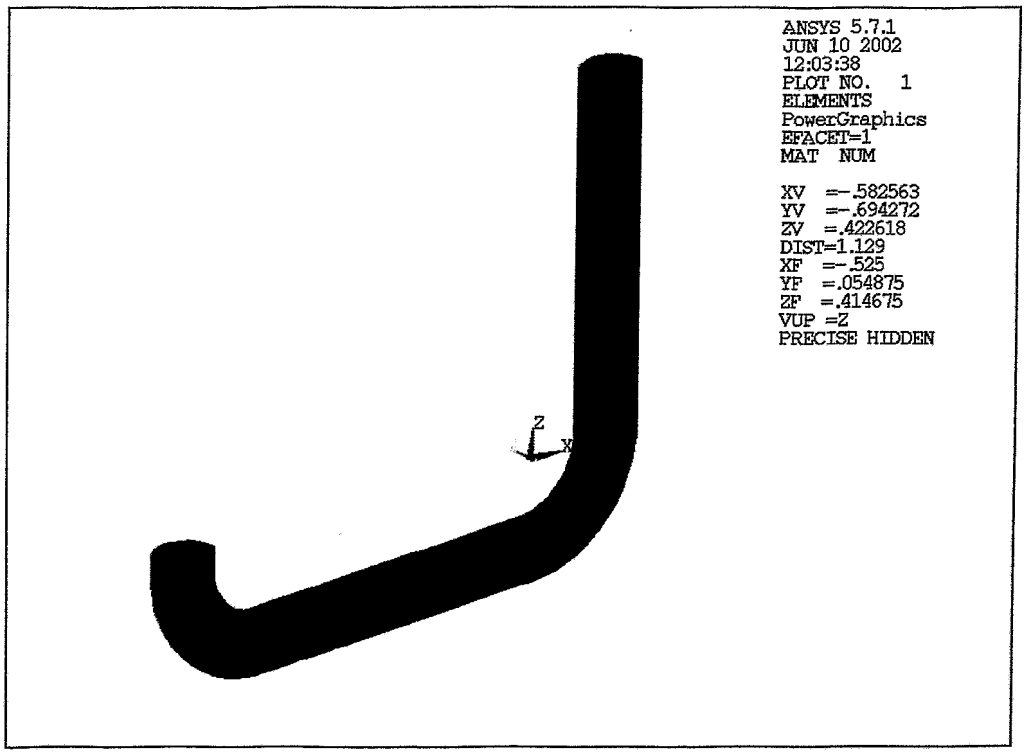

Figure 39: 3D FE-model of the CWHTF; red: pipe wall, blue: fluid

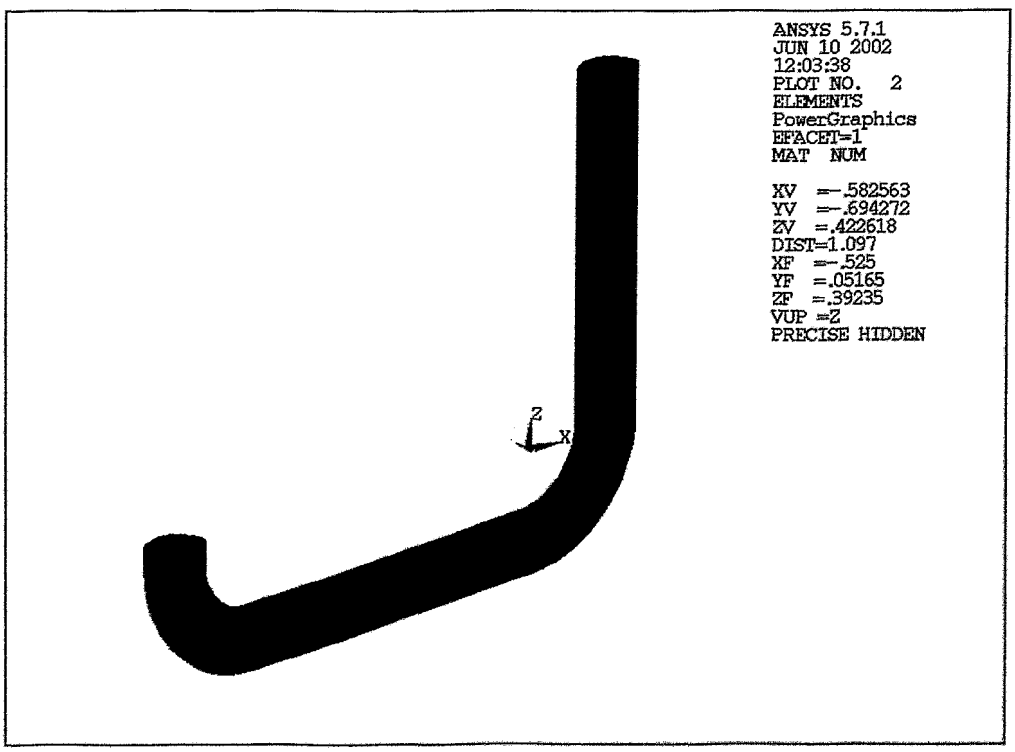

Figure 40: 3D FE-model of the CWHTF; shell element cover (SHELL43)

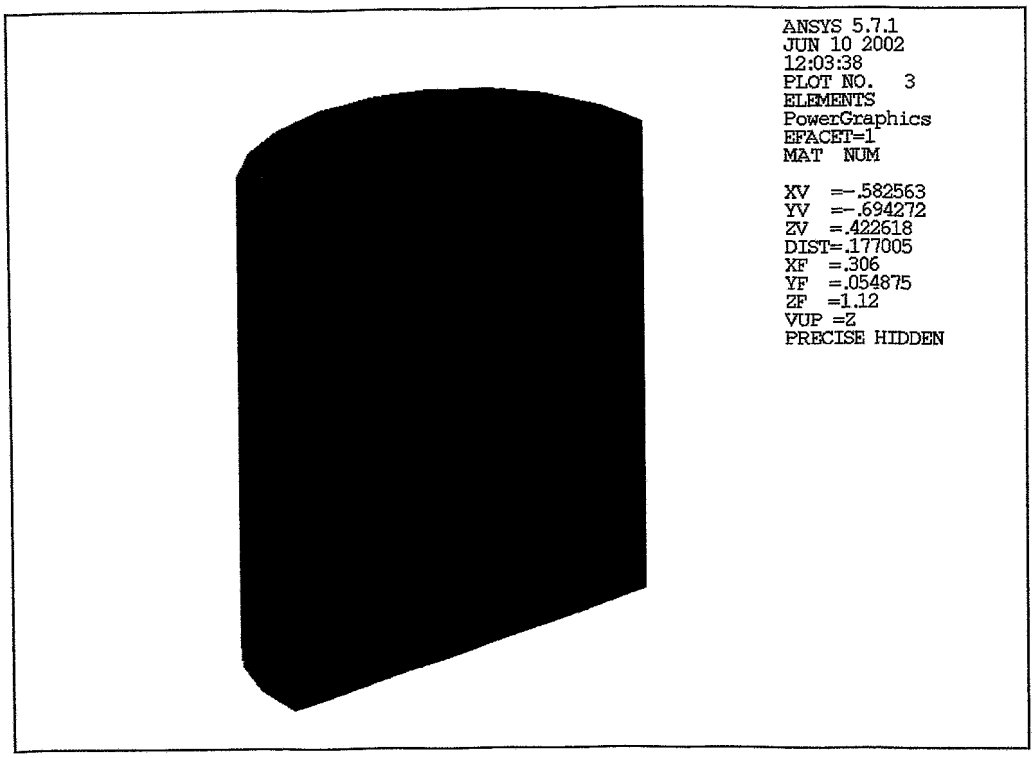

Figure 41: 3D FE-model of the CWHTF, bouncing plate region

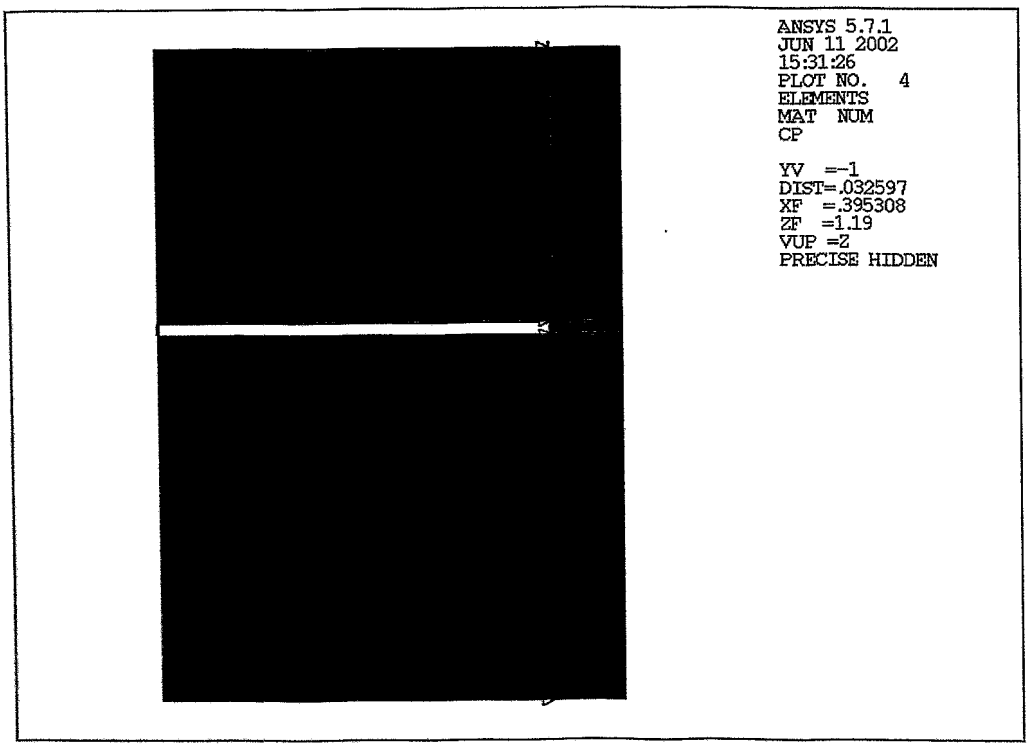

Figure 42: 3D FE-model of the CWHTF, coupling between the fluid elements and the structural elements; pink: rigid beams, green coupled DOFs

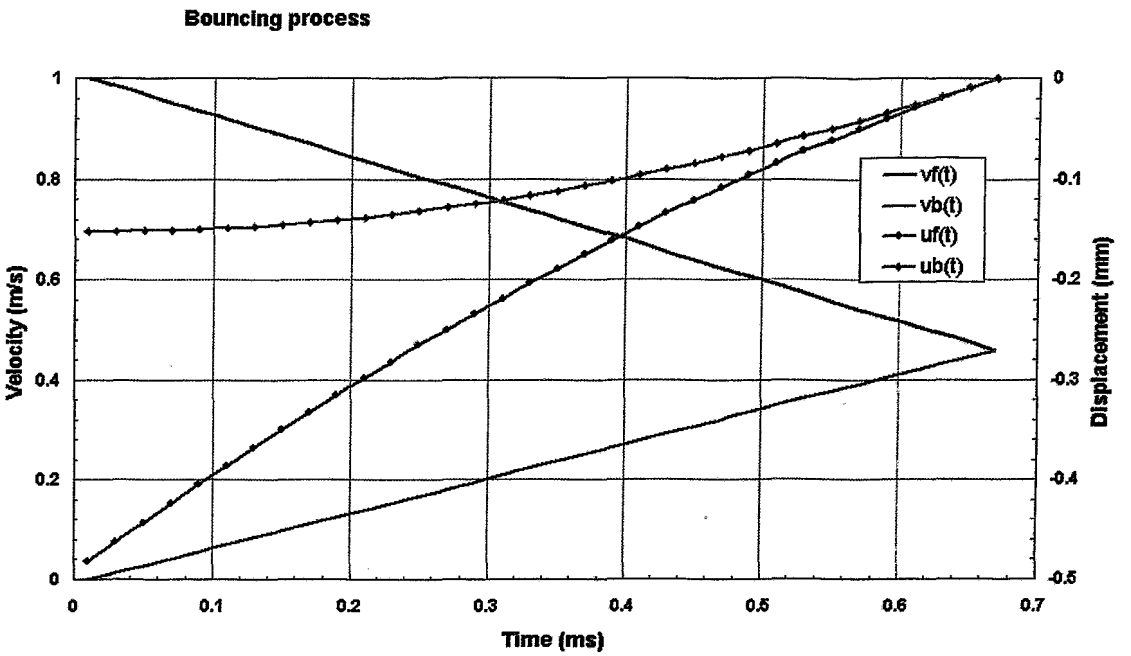

Figure 43: Velocity [m/s] and displacement [mm] of fluid front and bouncing plate during the bouncing process; initial fluid velocity $v_{F0} = 1$ m/s; steam collapse time $t_c = 0.66$ ms

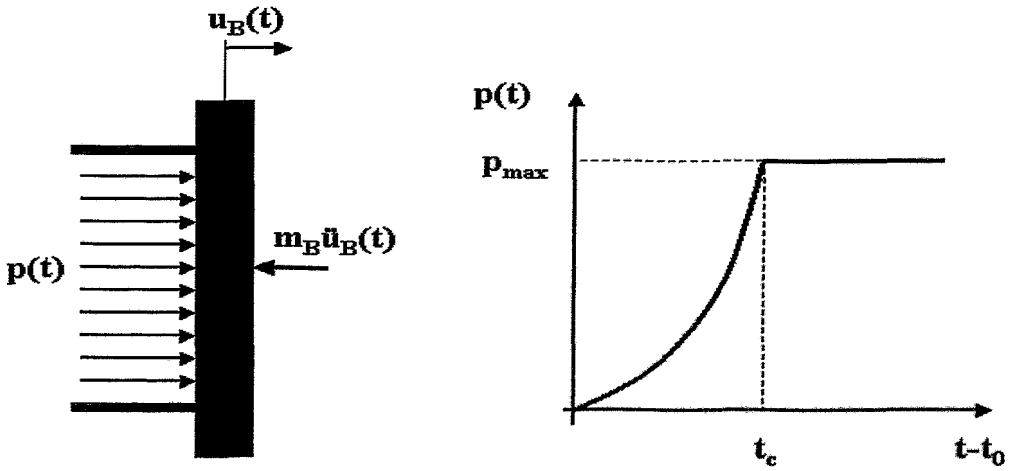

Figure 44: Model for the calculation of the bouncing plate velocity after bouncing: $v_B(t_0+t_c) = v_c$, n=2

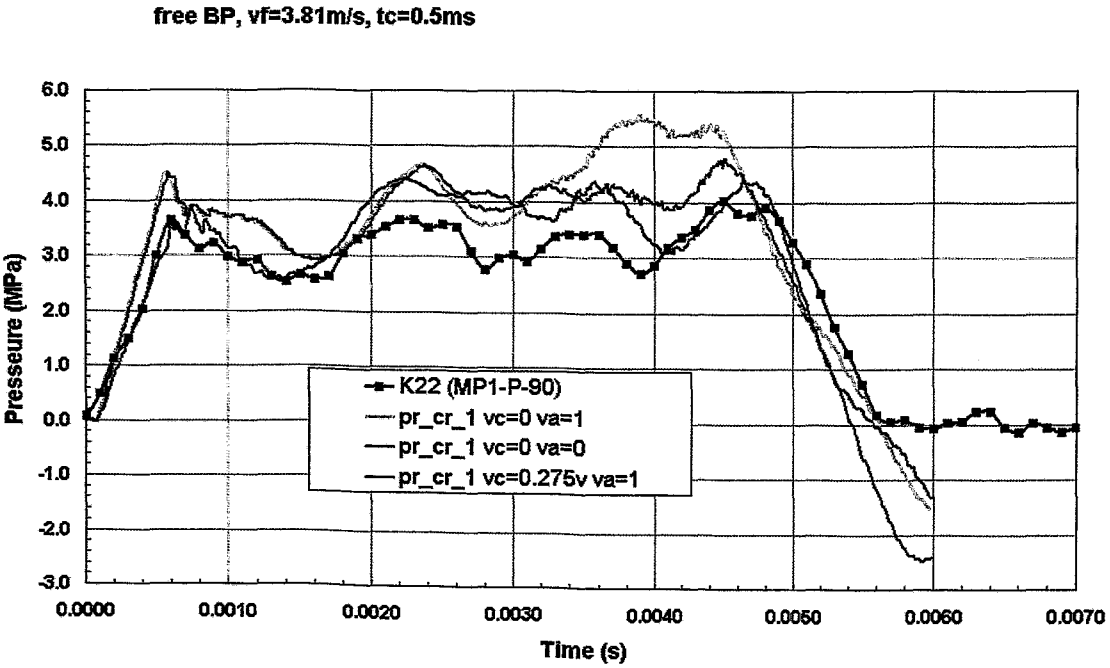

Figure 45: Test case 290601. Comparison of pressures at MP1; experiment (K22), simulation with fixed valve and v_c=0 (pr_cr_1 vc=0 va=1), simulation with free valve and v_c =0 (pr_cr_1 vc=0 va=0) and simulation with free valve and $v_c = 0.275v_F$ (pr_cr_1 vc=0.275v va=0)

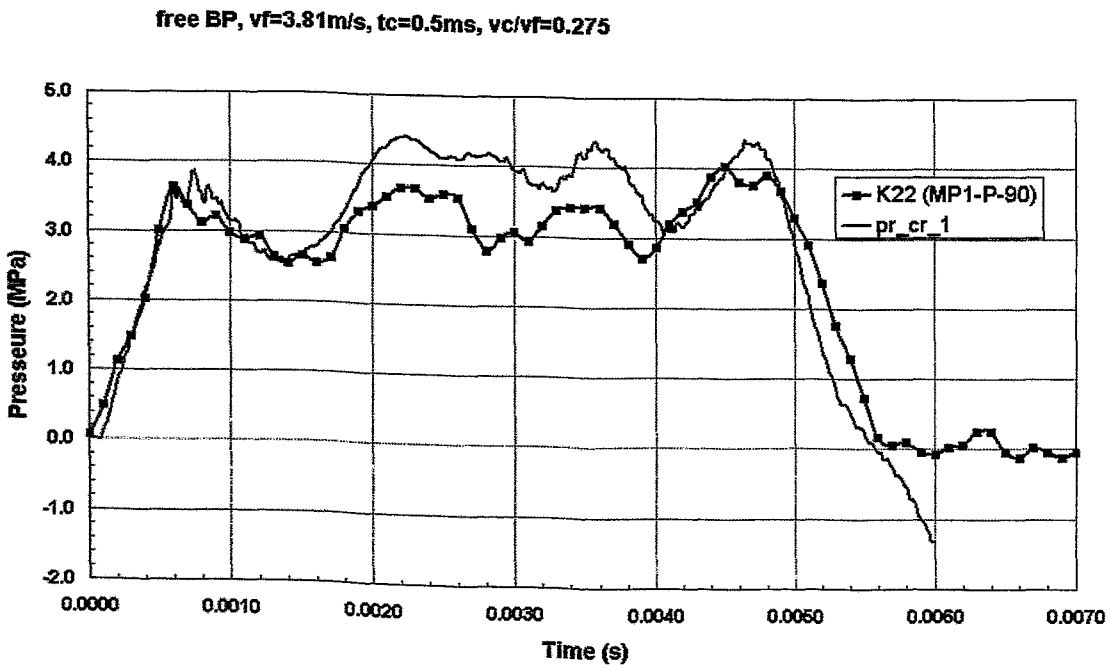

Figure 46: Test case 290601. Comparison of pressures at MP1; experiment (K22), simulation with free valve and v_c=$0.275v_F$ (pr_cr_1)

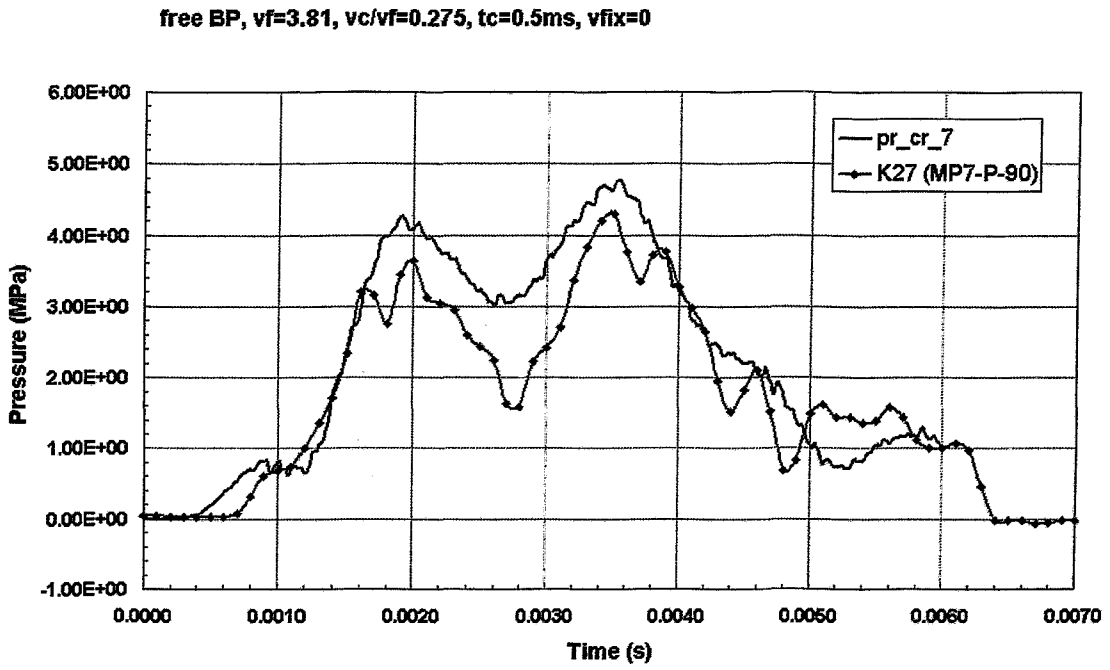

Figure 47: Test case 290601. Comparison of pressures at MP7; experiment (K27), simulation with free valve and $v_c=0.275v_F$ (pr_cr_7)

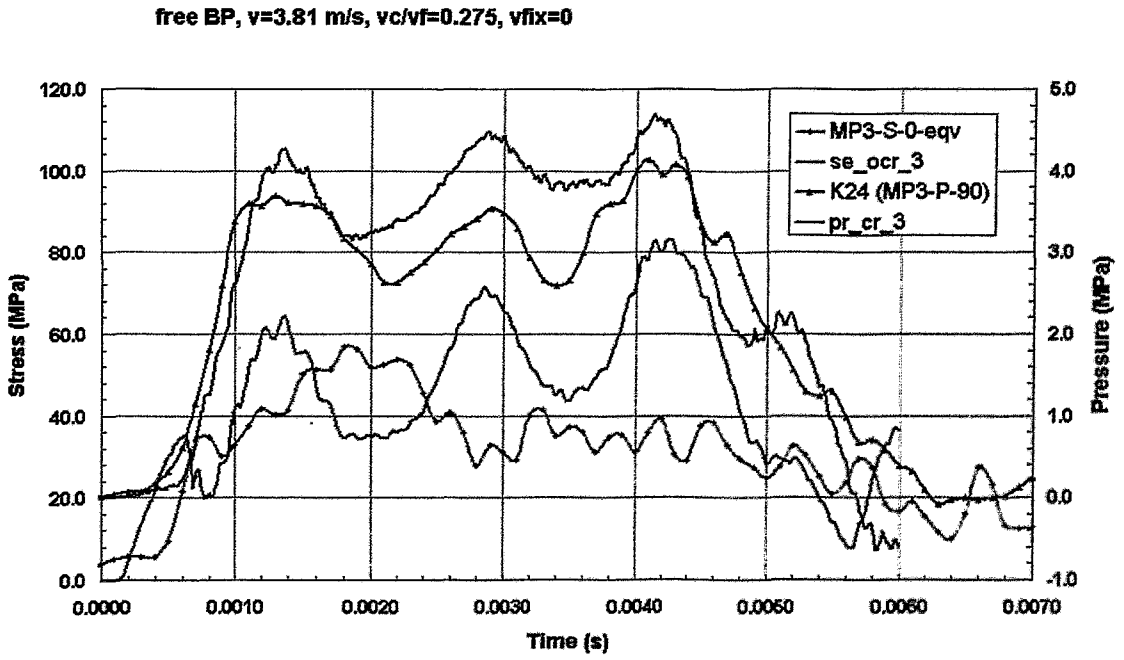

Figure 48: Test case 290601. Comparison of pressures (blue) and equivalent stresses (red) at MP3; experiment (K24 and MP3-S-0-eqv), simulation with free valve and $v_c=0.275v_F$ (pr_cr_3 and se_ocr_3)

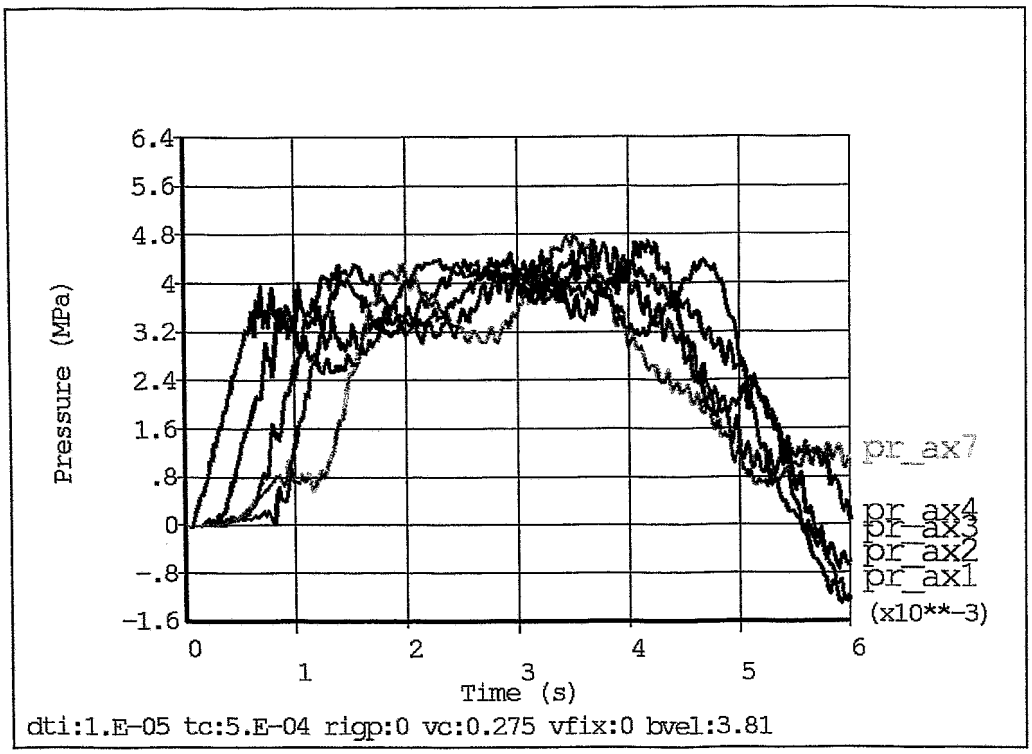

Figure 49: Test case 290601; Pressures (MPa) over time on the axis at MP1,2,3,4,7

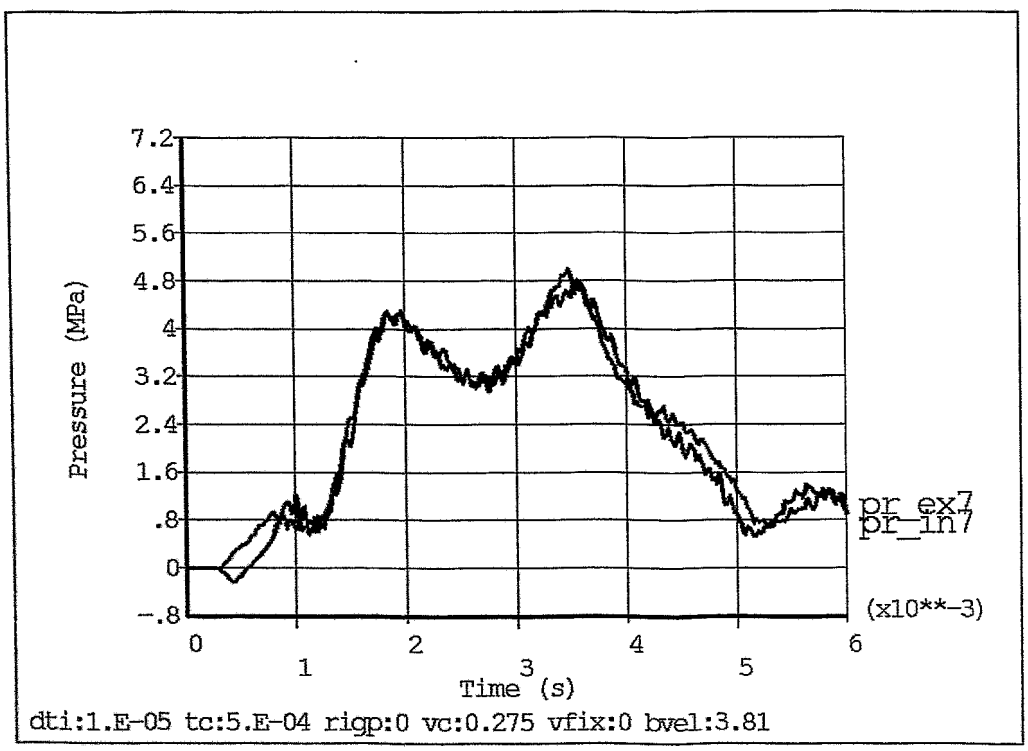

Figure 50: Test case 290601; Pressures (MPa) over time at MP7 intrados and extrados

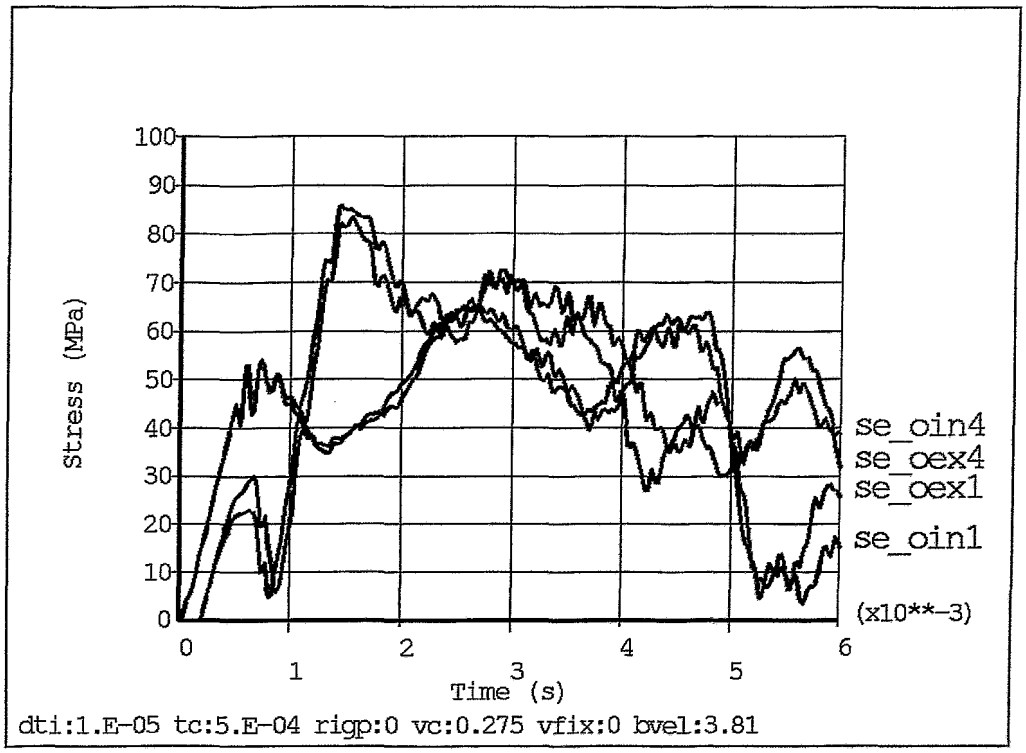

Figure 51: Test case 290601; Equivalent stresses (MPa) over time at MP1 and MP4 (outer wall side, extrados and intrados)

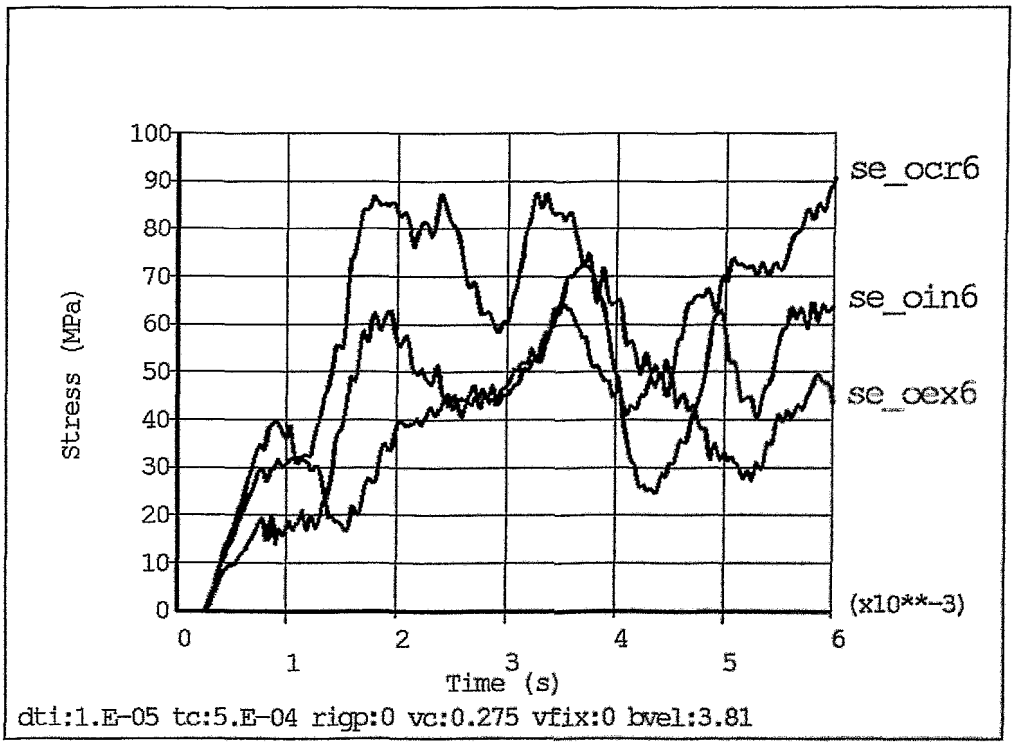

Figure 52: Test case 290601; Equivalent stresses (MPa) over time at MP6 (outer wall side, extrados, crown and intrados)

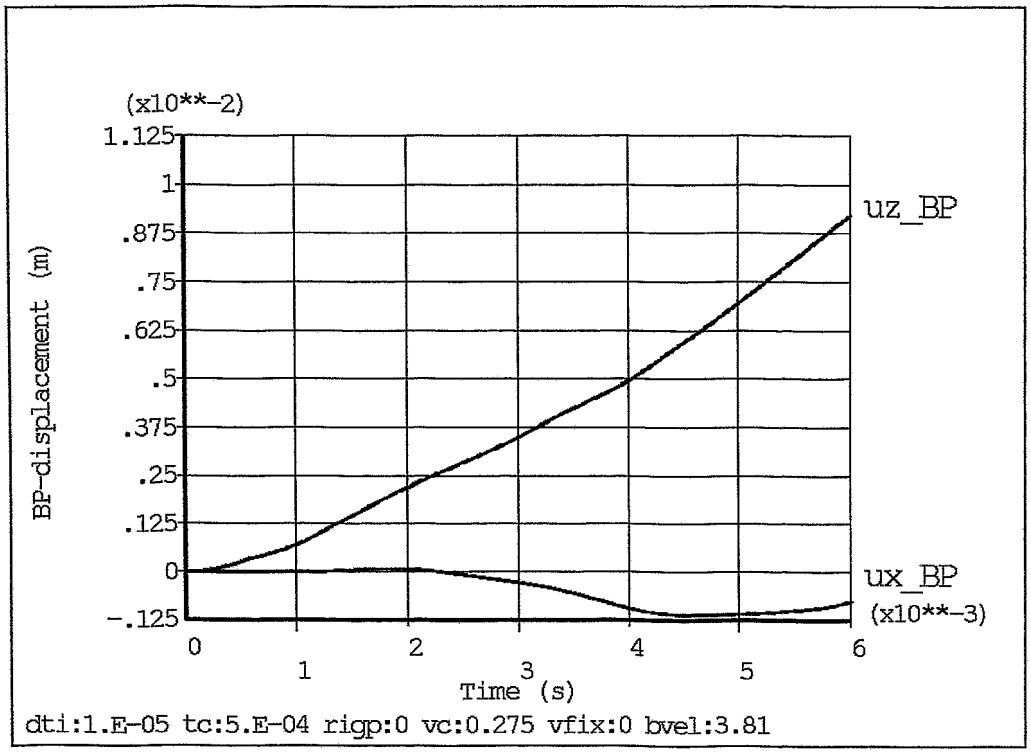

Figure 53: Test case 290601; bouncing plate displacement (m) over time

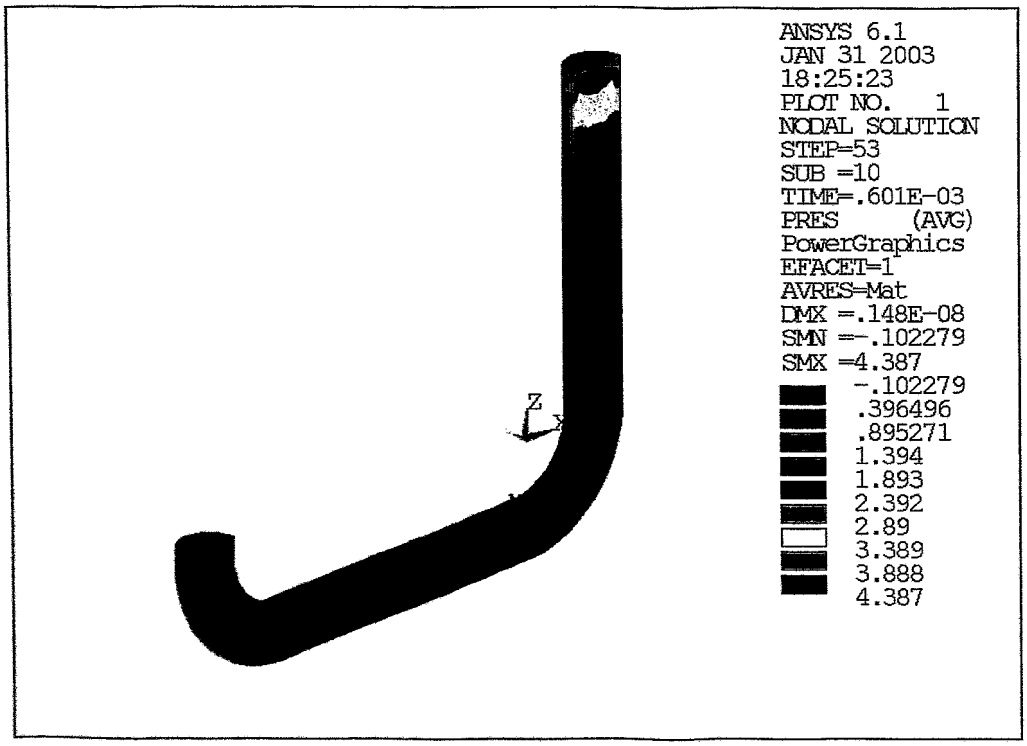

Figure 54: Test case 290601; Pressure distribution (MPa) at t=0.6 ms

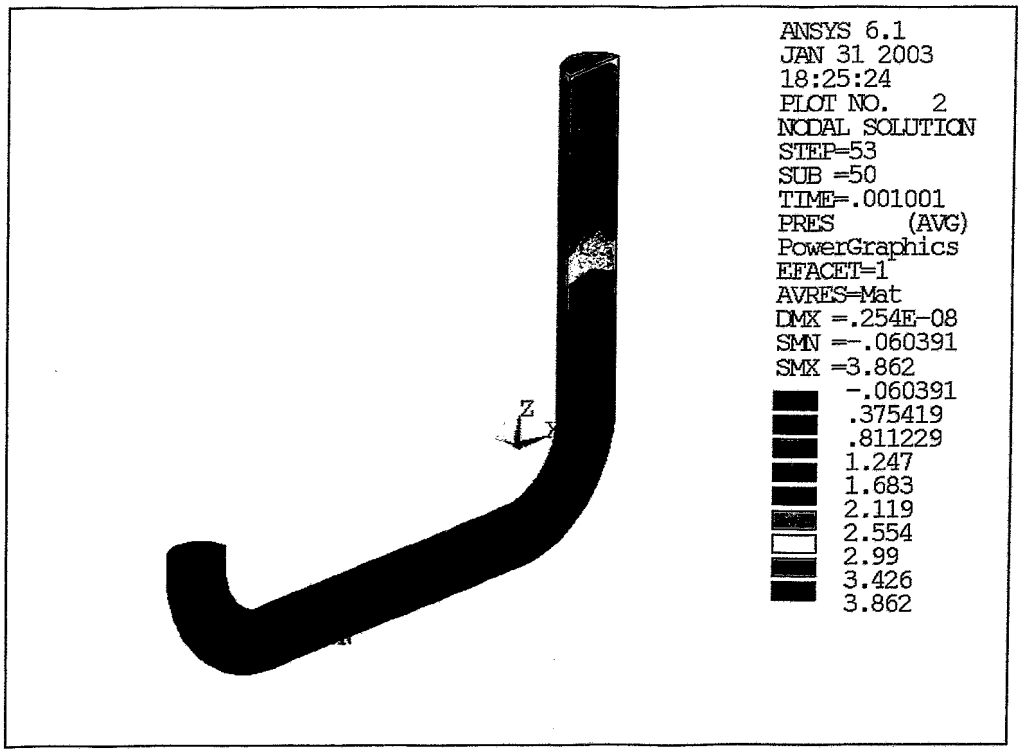

Figure 55: Test case 290601; Pressure distribution (MPa) at t=1 ms

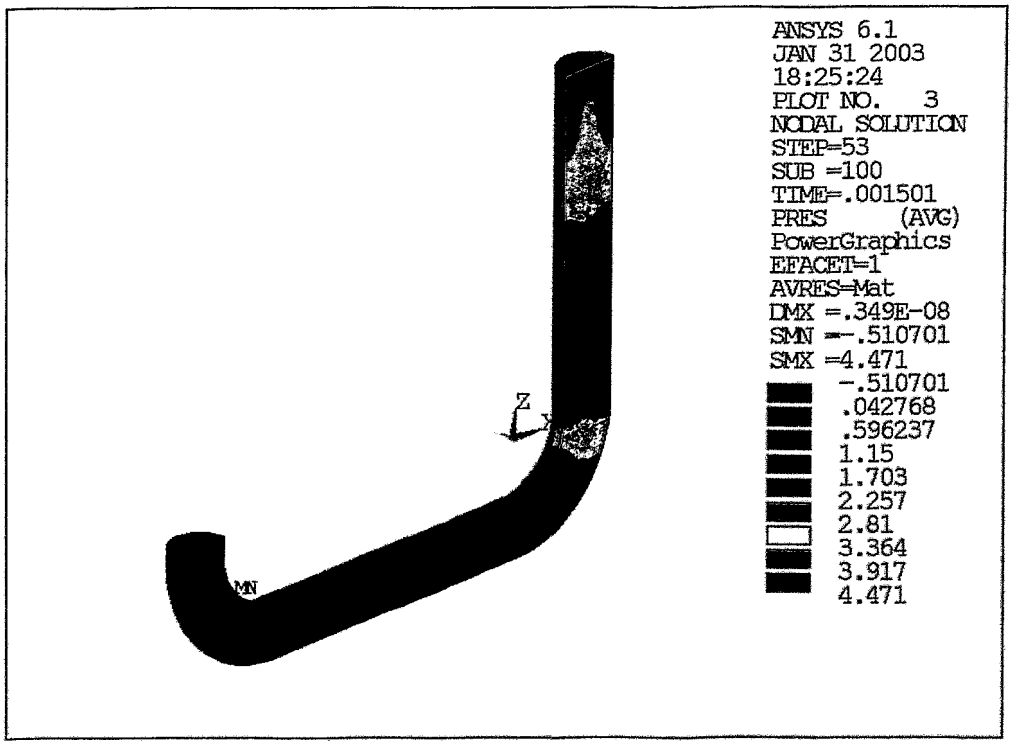

Figure 56: Test case 290601; Pressure distribution (MPa) at t=1.5 ms

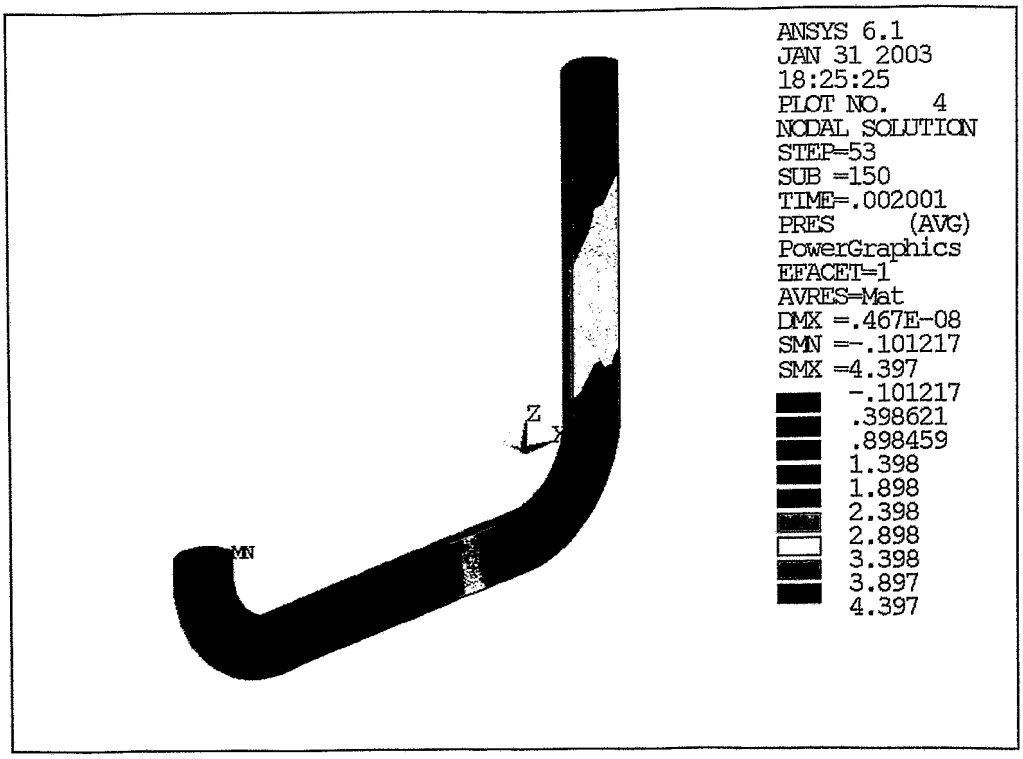

Figure 57: Test case 290601; Pressure distribution (MPa) at t=2 ms

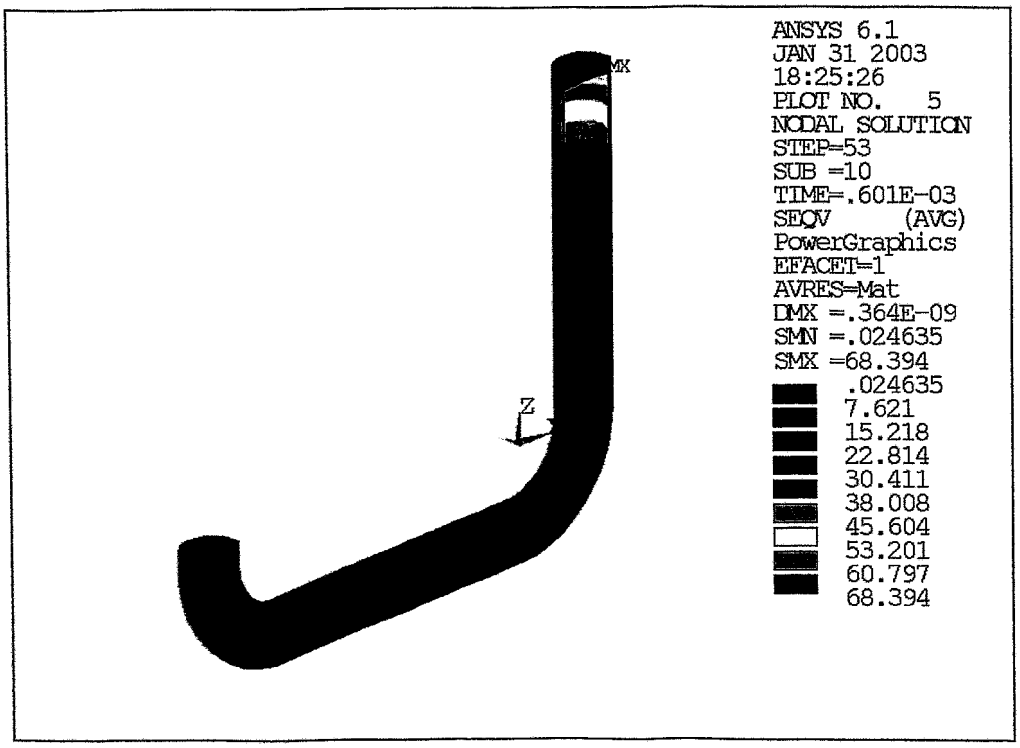

Figure 58: Test case 290601; Stress distribution (MPa) at t=0.6 ms

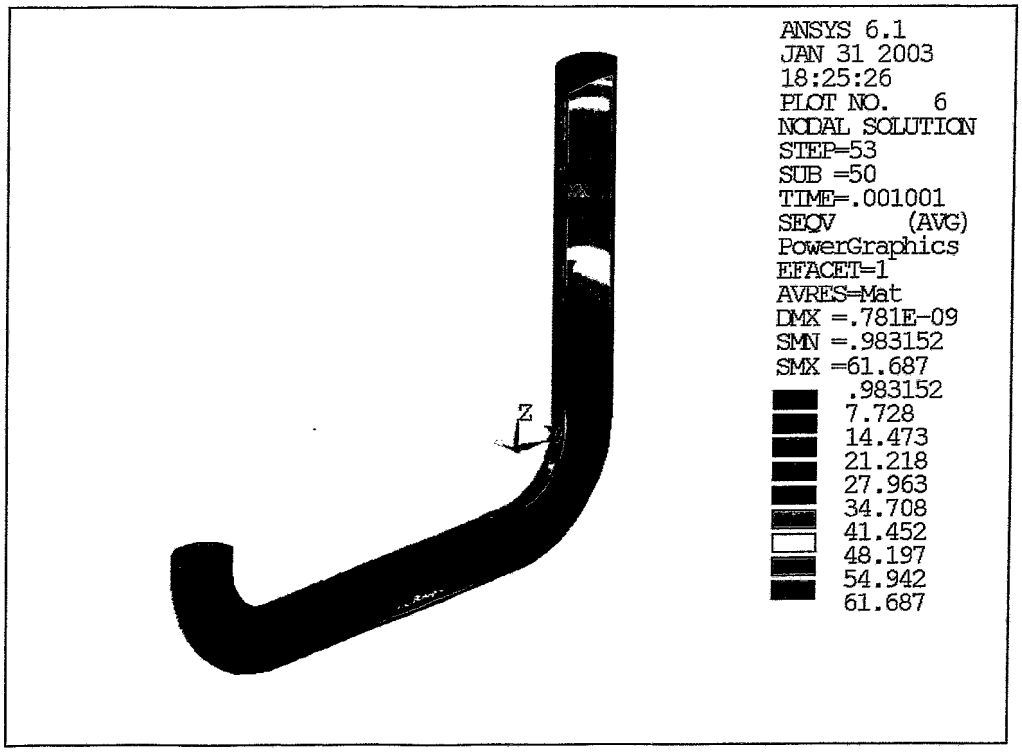

Figure 59: Test case 290601; Stress distribution (MPa) at t=1 ms

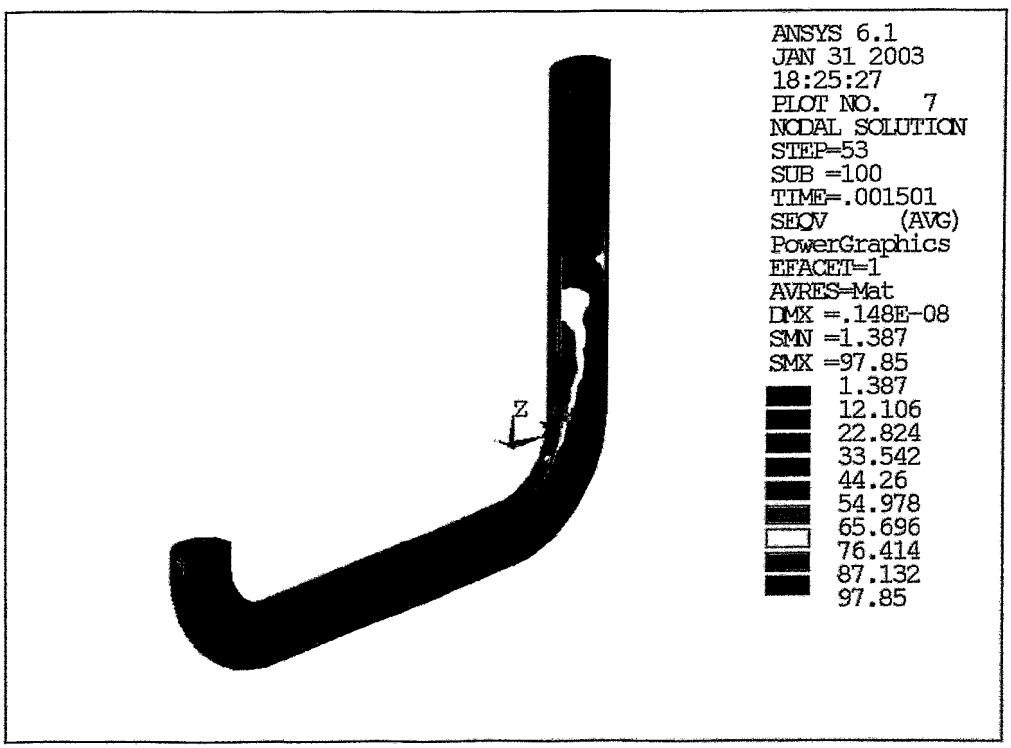

Figure 60: Test case 290601; Stress distribution (MPa) at t=1.5 ms

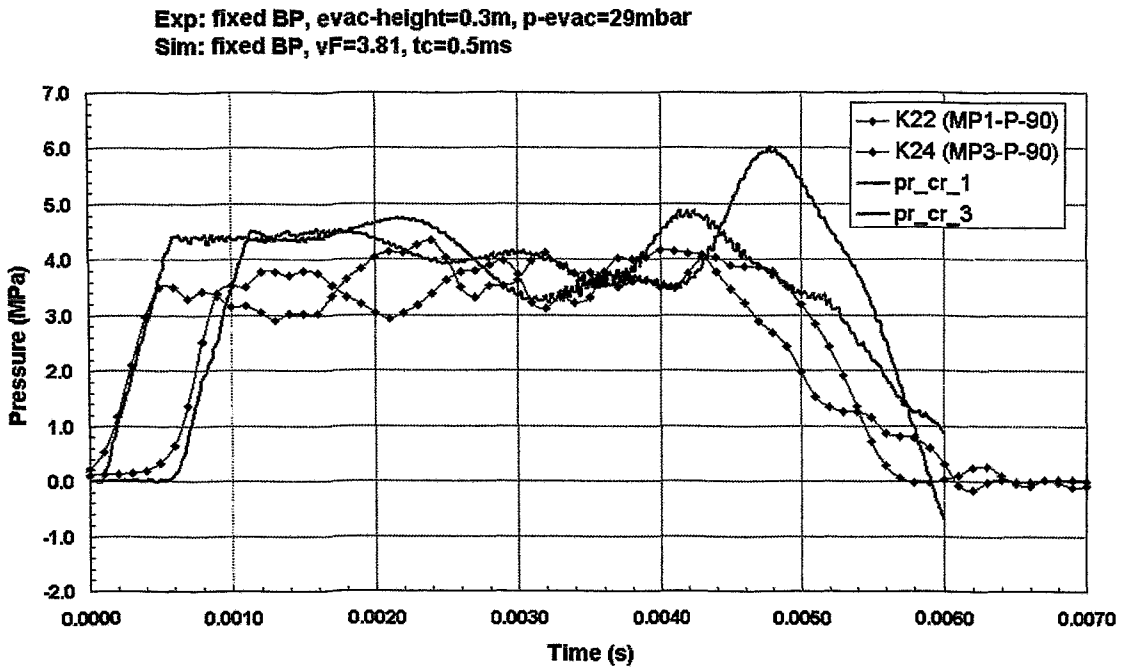

Figure 61: Test case 190601. Comparison of pressures at MP1 and MP3; experiment (K22, K24), simulation with fixed bouncing plate (pr_cr_1 and pr_cr_3)

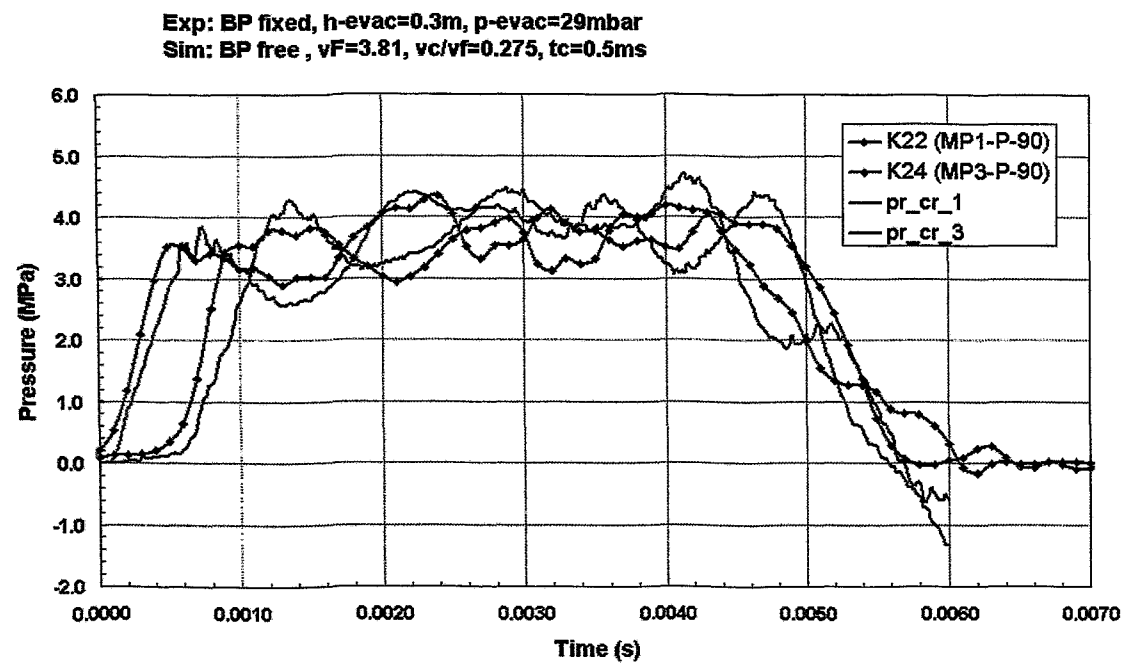

Figure 62: Test case 190601. Comparison of pressures at MP1 and MP3; experiment (K22, K24), simulation with free bouncing (pr_cr_1 and pr_cr_3)

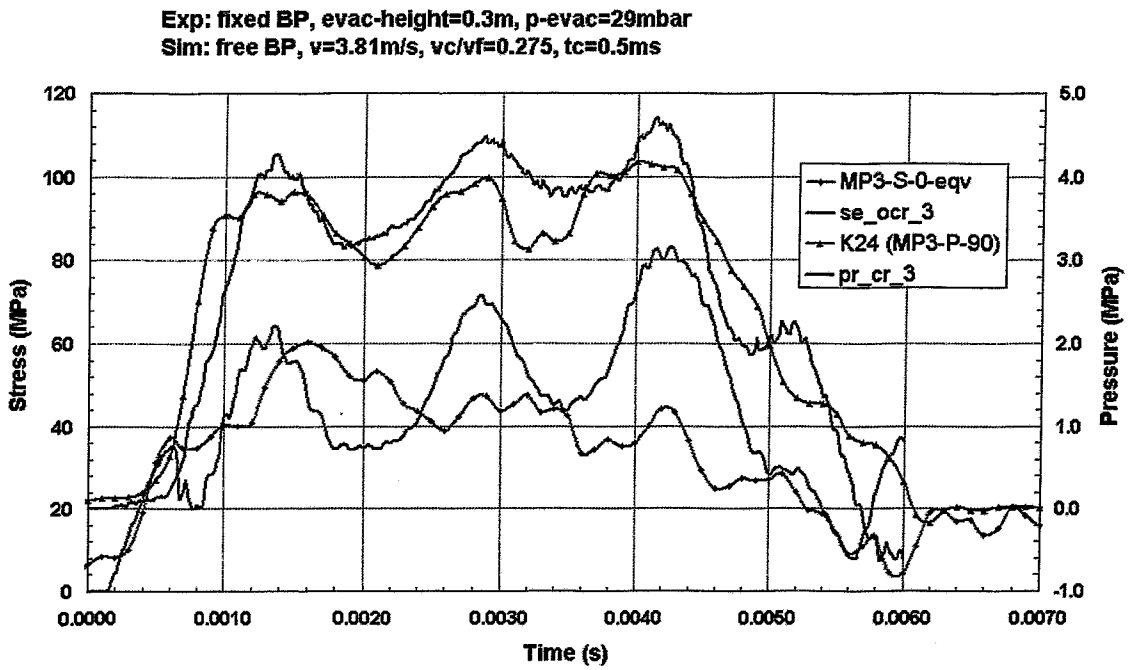

Figure 63: Test case 190601. Comparison of pressures (blue) and equivalent stresses (red) at MP3; experiment (K24 and MP3-S-0-eqv), simulation with free valve and $v_c=0.275v_F$ (pr_cr_3 and se_ocr_3)

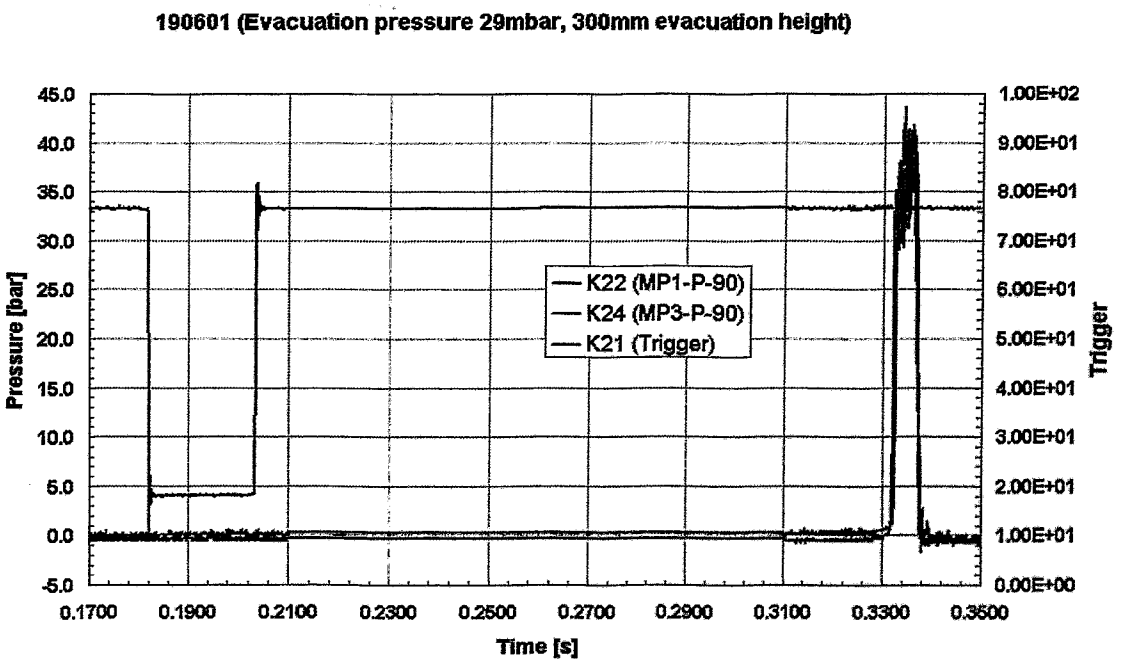

Figure 64: Test case 190601. Pressure (experimental) over time and trigger signal (valve opening). The difference between valve opening is about 0.151 s

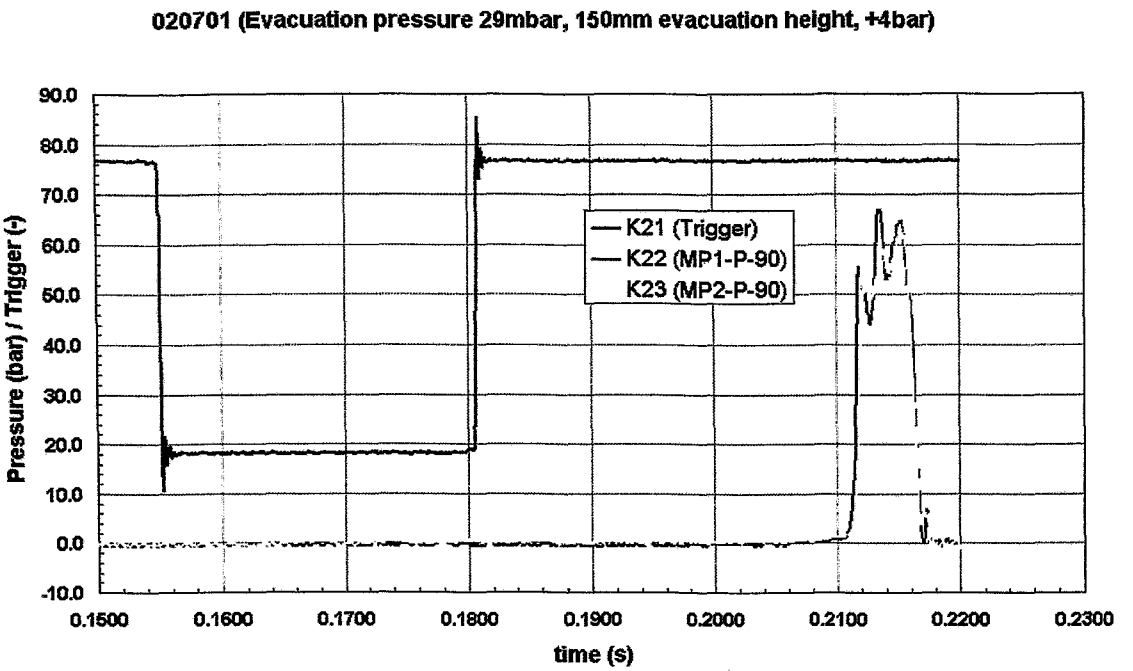

Figure 65: Test case 020701. Pressure (experimental) over time and trigger signal (valve opening). The difference between valve opening is about 0.056 s

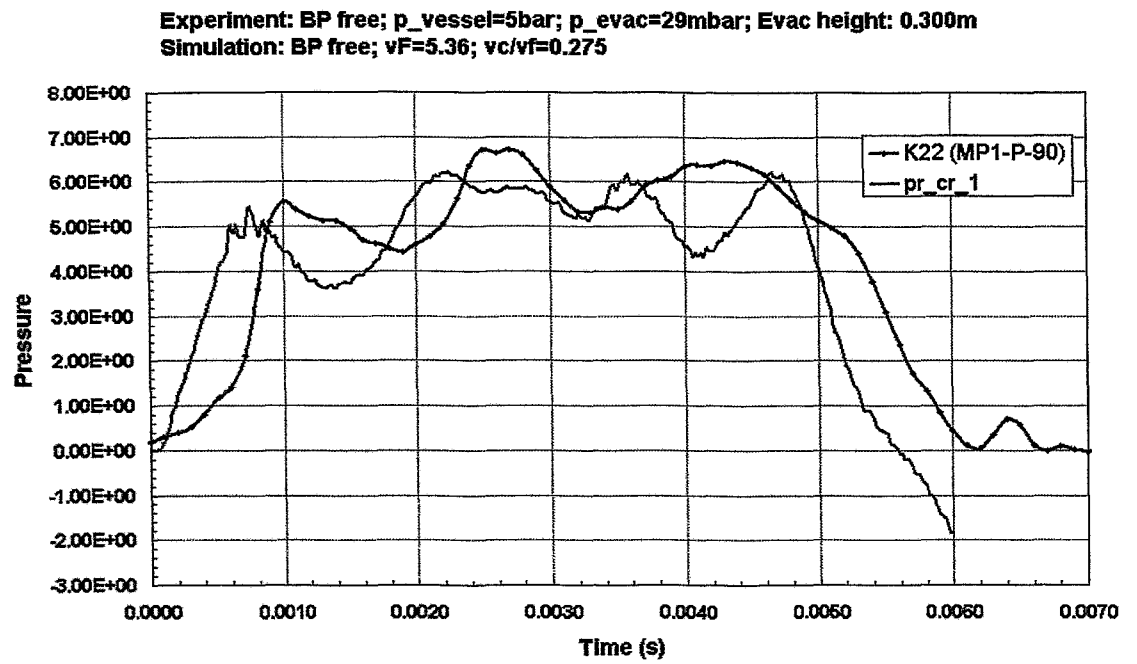

Figure 66: Test case 190601. Comparison of pressures (MPa) at MP1; experiment (K22), simulation with free valve and $v_c=0.275v_F$ (pr_cr_1)

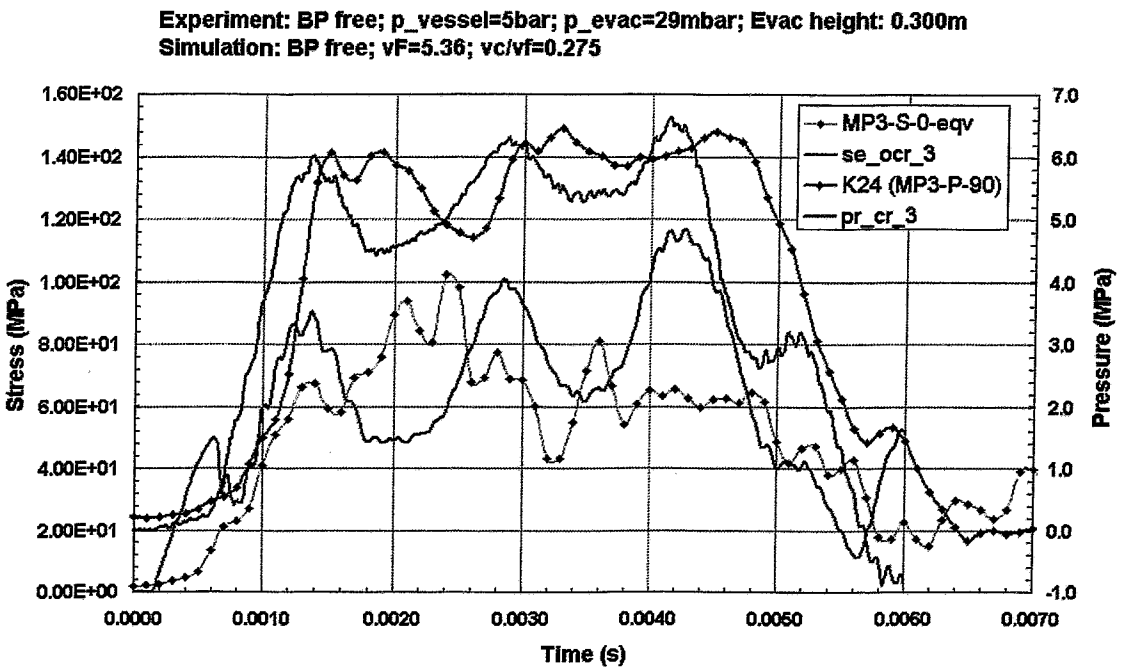

Figure 67: Test case 020701. Comparison of pressures (blue) and equivalent stresses (red) at MP3; experiment (K24 and MP3-S-0-eqv), simulation with free valve and $v_c=0.275v_F$ (pr_cr_3 and se_ocr_3)

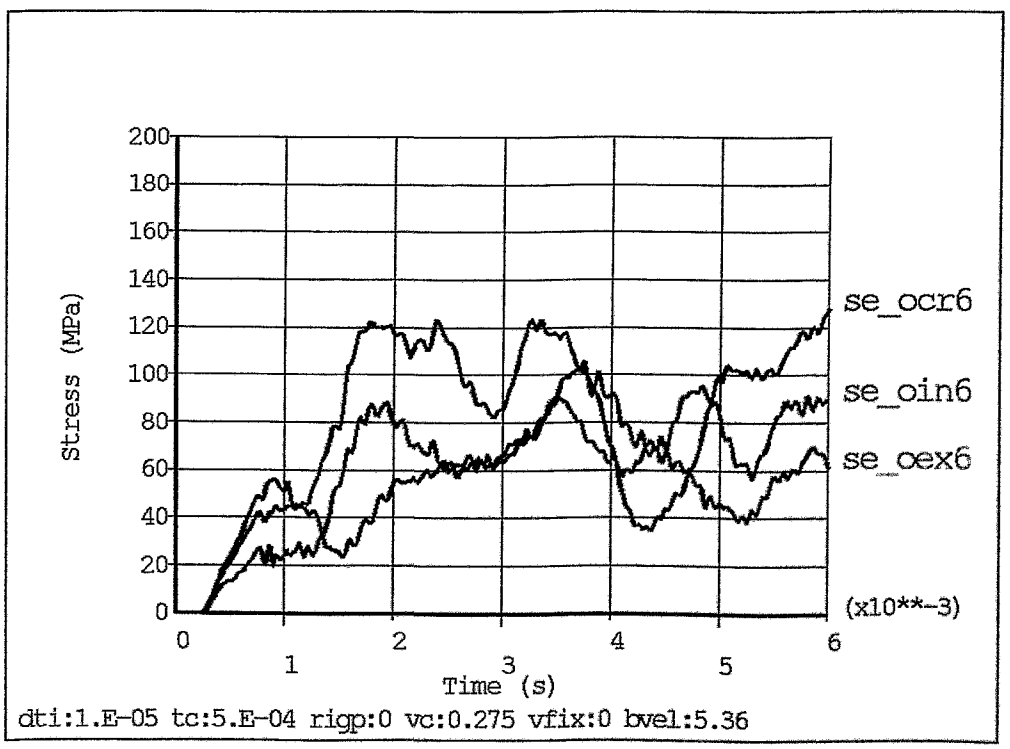

Figure 68: Test case 020701; Equivalent stresses (MPa) over time at MP6 (outer wall side, extrados, crown and intrados)

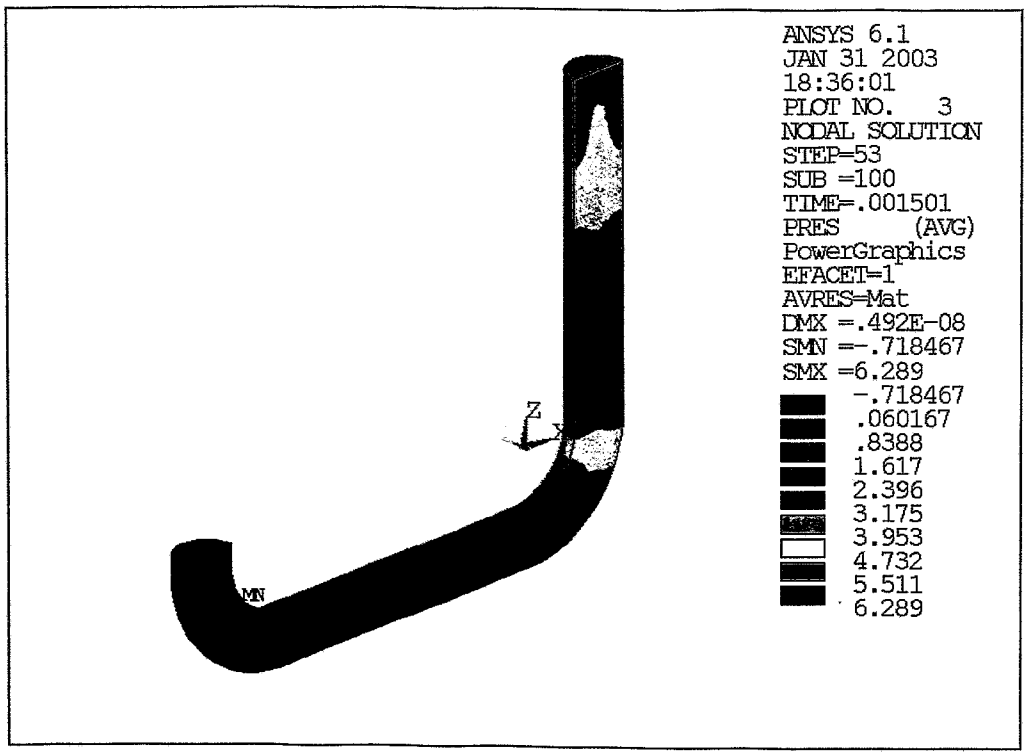

Figure 69: Test case 020701; Pressure distribution (MPa) at t=0.0015 s

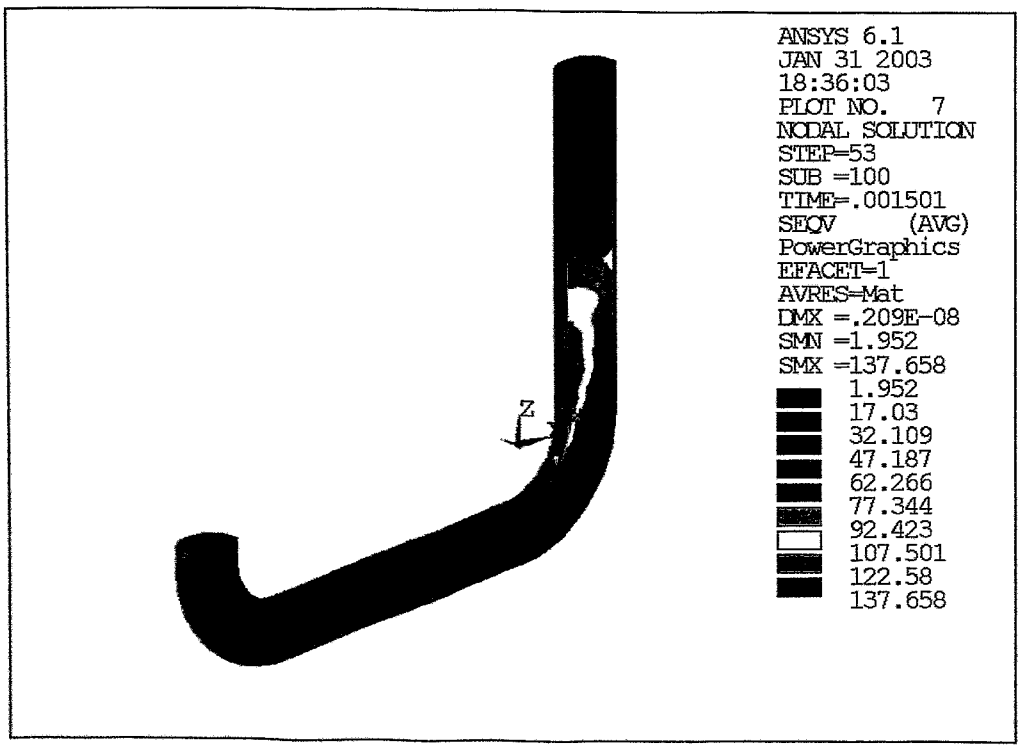

Figure 70: Test case 020701; Stress distribution (MPa) at t=0.0015 s

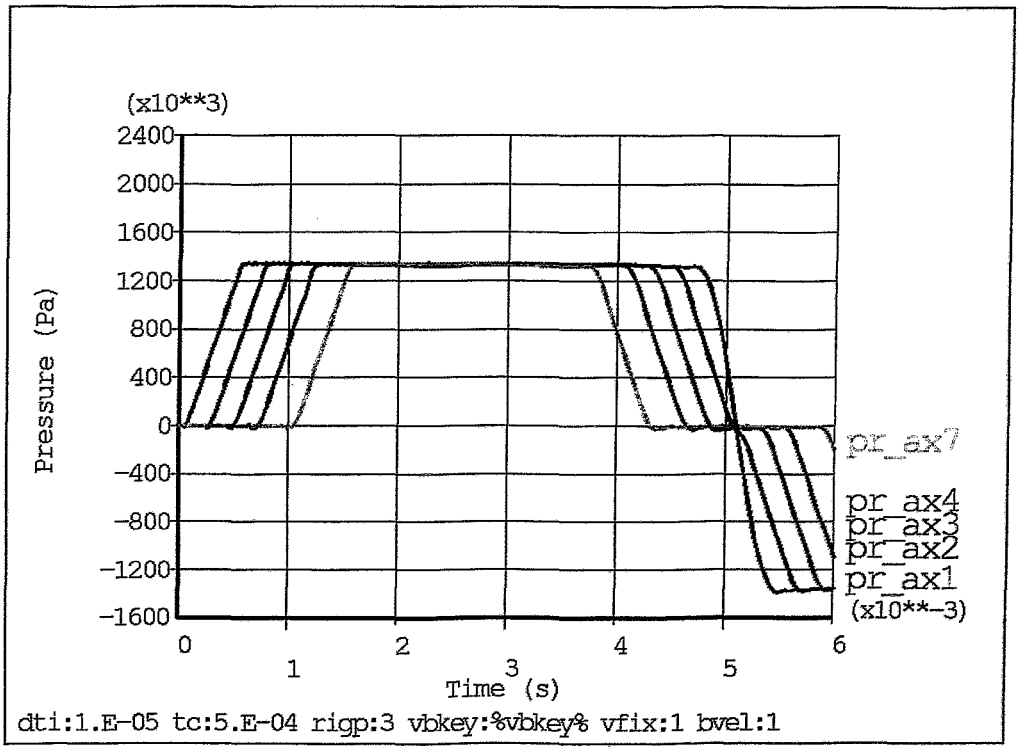

Figure 71: Simulation of rigid pipe with $v_F = 1.0$ m/s; Pressure over time on the axis at MP1,2,3,4,7

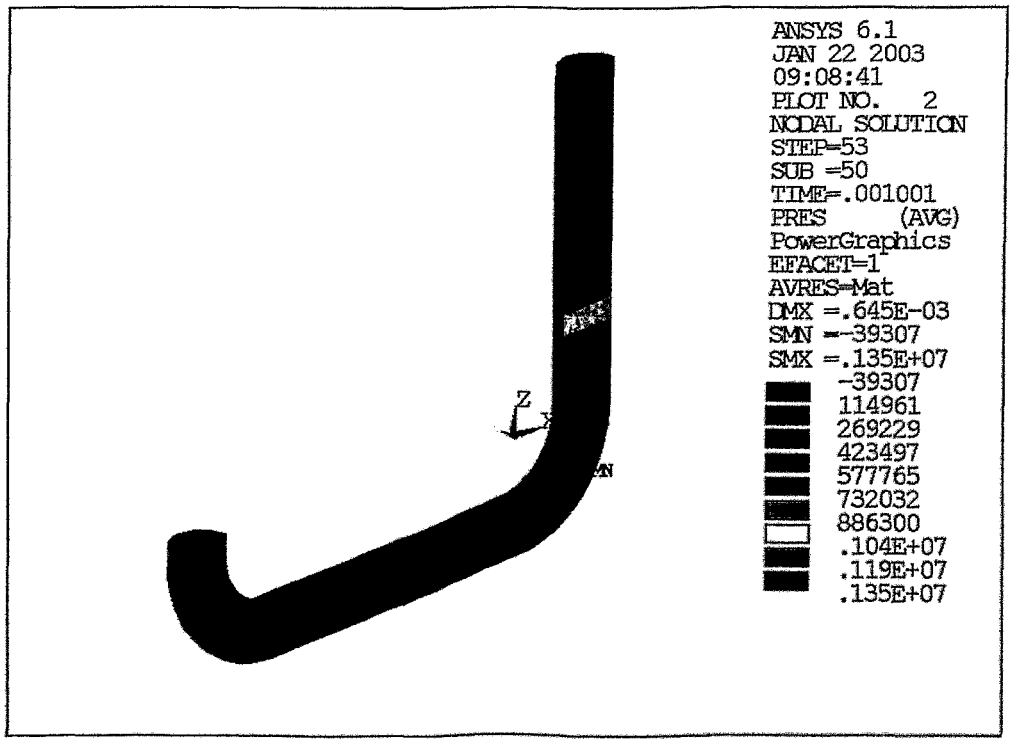

Figure 72: Simulation of rigid pipe with $v_F = 1.0$ m/s; Pressure distribution (Pa) at t = 0.001 s

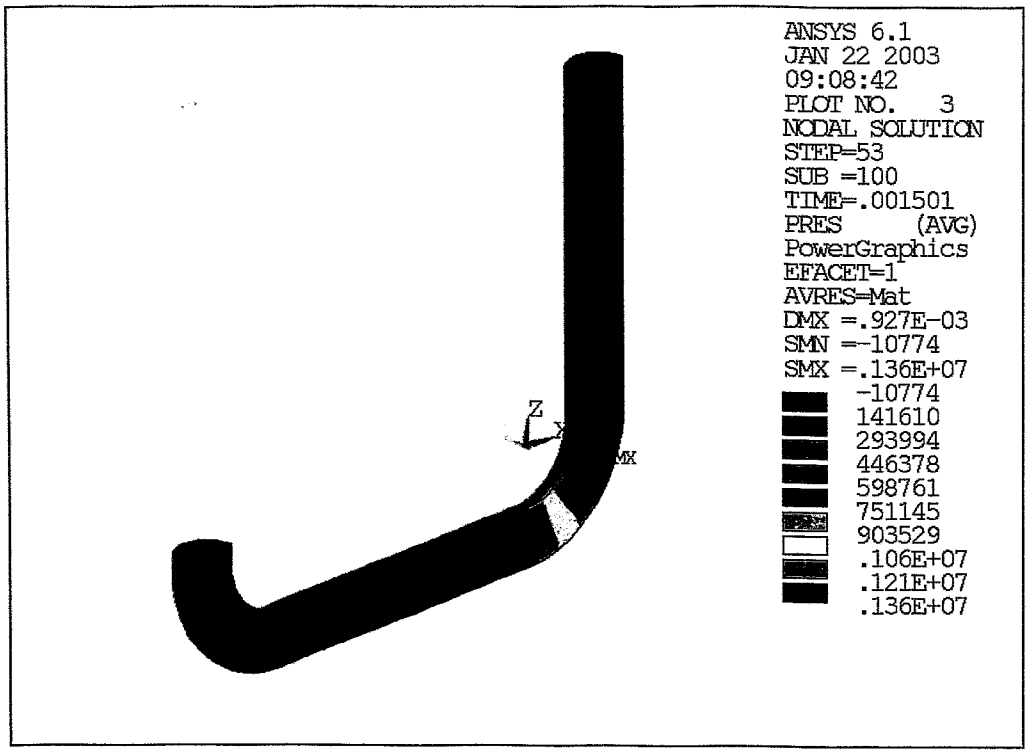

Figure 73: Simulation of rigid pipe with $v_F = 1.0$ m/s; Pressure distribution (Pa) at t = 0.0015 s

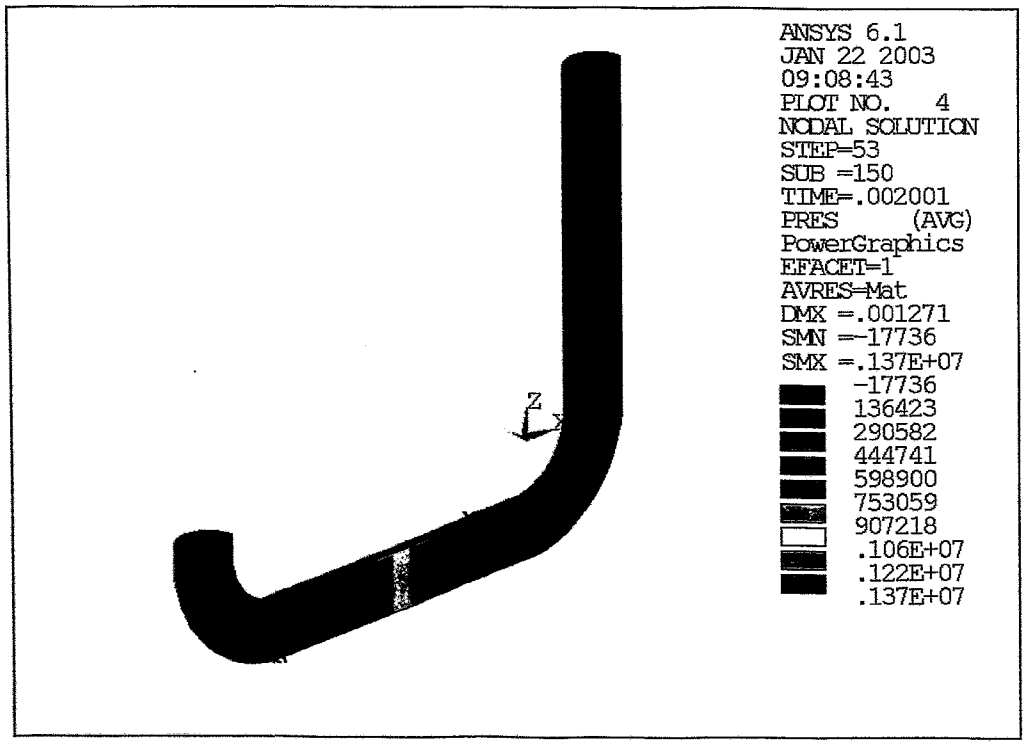

Figure 74: Simulation of rigid pipe with $v_F = 1.0$ m/s; Pressure distribution (Pa) at t = 0.002 s